2010

REAL TIME 3-D TRACKING OF THE HIGH DOSE RATE RADIATION SOURCE USING A FLAT PANEL DETECTOR

Aditya Bondal
Virginia Commonwealth University

REAL TIME 3-D TRACKING OF THE HIGH DOSE RATE RADIATION SOURCE

USING A FLAT PANEL DETECTOR

A thesis submitted in partial fulfillment of the requirements for the degree of Master of Science at Virginia Commonwealth University.

by

ADITYA BONDAL
Bachelor of Engineering, Mumbai University, India 2006

Director: DORIN TODOR, PH.D.
ASSOCIATE PROFESSOR, RADIATION ONCOLOGY

Director: DING-YU FEI, PH.D.
ASSOCIATE PROFESSOR, BIOMEDICAL ENGINEERING

Virginia Commonwealth University
Richmond, Virginia
August, 2010

Acknowledgement

Firstly, I would like to thank my research advisor and mentor, Dr. Dorin Todor, who has supported me throughout my thesis with his patience, knowledge and occasional humor. I attribute the level of my Masters degree to his encouragement and effort and without him this thesis, would not have been completed or written.

I would also like to thank Dr Ding-Yu Fei for being my academic advisor and guiding me with course work and my research. His unconditional guidance and support during the Biomedical Instrumentation and Imaging class helped me understand crucial concepts essential for my project and ultimately my thesis.

I would like to thank Dr Ou Bai for agreeing to be on my master's defense committee.

I am very grateful to Dr Williamson for providing financial support during my masters and giving me the opportunity to work with Dr Todor.

I am extremely thankful to Chris, Lynn, Tatjana and Chem for helping me operate the Acuity machine. Without you guys I would have no data to play around with.

Most importantly I would like to thank my family. Without their love and support none of this would have been possible. My dad Ashwin Bondal, who has been the one person I look up to, my role model and one day I hope to be just like him and my mom Kumud Bondal who raised me to be the man I am today, I dedicate this thesis to the two

of you. I would also like to thank my sister for being there when I missed my family and supporting me in every possible way.

Last but not least I would like to thank all my friends in Richmond and as well as back home who have always been there during my ups and downs in life. Especially my friends in Richmond for being my family away from home, thanks guys. Above all, I would like to thank God for helping me in every walk of life.

Table of Contents

Page

List of Tables

Page

List of Figures

Page

List of Abbreviations

APBI – Accelerated Partial Breast Irradiation

BCS – Breast Conservation Surgery

CT – Computed Tomography

DHI – Dose Homogeneity Index

EBRT – External beam radiation therapy

FPD – Flat Panel Detector

HDR – High Dose Rate

MIB – Multicatheter Interstitial Brachytherapy

RT – Radiation Therapy

TPS – Treatment Planning System

QA – Quality Assurance

Abstract

REAL TIME 3D TRACKING OF THE HIGH DOSE RATE RADIATION SOURCE

USING A FLAT PANEL DETECTOR

By Aditya Bondal, B.E.

A Thesis submitted in partial fulfillment of the requirements for the degree of Masters of Science at Virginia Commonwealth University.

Virginia Commonwealth University, 2010

Major Director: Dorin Todor, Ph.D.
Associate Professor, Radiation Oncology

A number of QA procedures have been developed for Breast Brachytherapy treatments, yet none guarantee accurate dose delivery or allow conformation of the actual source position leading to errors sometimes going unnoticed. The objective of this study is to track the exact path the HDR source would follow in real time. The exit radiation of the HDR source was used to image a well defined matrix of markers. The images were acquired using FPD and were processed to obtain projection coordinates while an x-ray calibration image was processed to obtain marker coordinates. Each marker along with its

projection represents a line in 3D. A mathematical solution for the 'near-intersection' of two 3D lines was implemented and used to determine the 'true' 3D source position. A matrix with N markers will produce N*(N-1)/2 points of intersection and their mean will result in a more accurate source position. This study has proved that the accuracy of source position detection using a FPD is sub-millimeter.

CHAPTER 1 Introduction

1.1 Background

Radiation Therapy (RT) has been used for over a century as a treatment for cancer[1]. Within a few years of the discovery of radium by the Curie's, the importance of the medical use of radioactive substances was realized, which lead to an increase interest in radiobiology and the beginning of brachytherapy[1]. Educating women against breast cancer through various health promotion campaigns has spread the awareness of the disease[2]. The 1980's and 1990's saw a sharp rise in the occurrence of early stage breast cancer that was tumors of less than 4cm in dimension being detected[3]. This was mainly due to the introduction and application of new breast cancer diagnostic techniques along with greater number of women obtaining mammography scans[4].

Breast brachytherapy is a Radiation Therapy procedure, which in the current era is typically delivered after lumpectomy as part of the breast conservation solution in Accelerated Partial Breast Irradiation (APBI) treatments. Brachytherapy as defined by the American Brachytherapy Society (ABS) is "the therapeutic use of encapsulated radionuclides within or close to a tumor[5]", that is the radiation source is placed within the tumor bed or in very close proximity to the area requiring treatment[6]. Brachytherapy is

derived from the Greek "brachios" which stands for short, as the radiation source is placed at very short distances from the tumor[5].

Lumpectomy is the surgical removal of only the part of the breast containing the cancer tumor[2,7]. Although the tumor is excised, microscopic residual of the tumor may exist on the borders of the tumor cavity. Radiation kills these microscopic residual thus reducing the chances of reoccurrence of the cancer tumor. A number of studies have proven that one of the most efficient radiation therapy methods for the treatment of breast cancer is Brachytherapy. Once the cancer tumor has been excised, catheters are inserted inside the area surrounding the tumor cavity in the breast (Figure 1)[8].

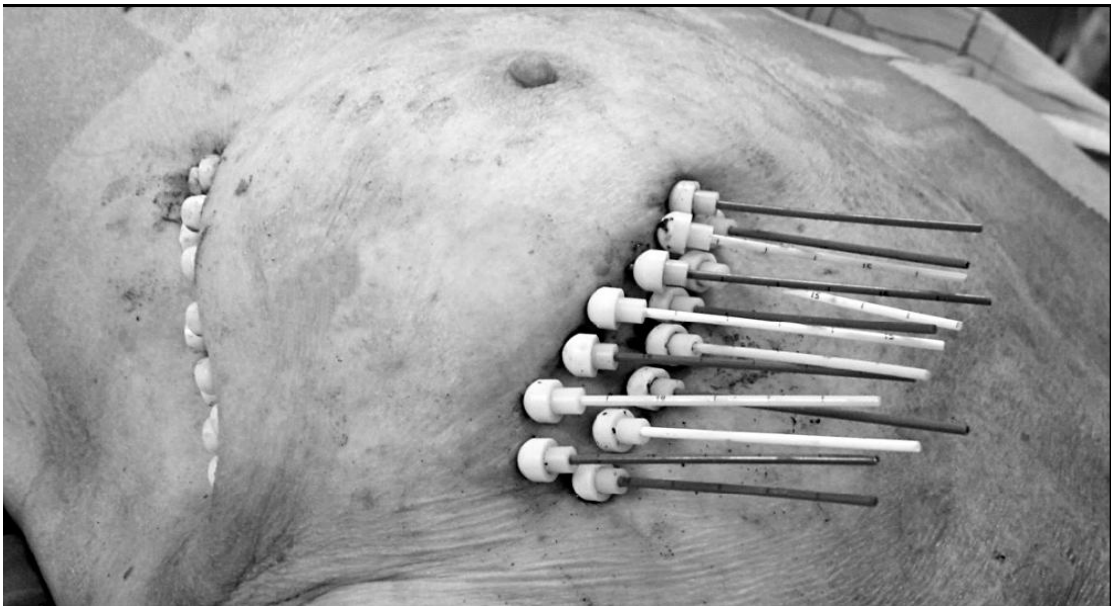

Figure 1: Multicatheter interstitial brachytherapy[8]

Catheters are cylindrical hollow tubes through which the radiation source can travel within the breast. The number of catheters depends on the size of the tumor. The catheters

are placed such that it assures optimal coverage to the radiation source of the target volume. Computed Tomography (CT) images of the catheters and the tumor cavity are acquired and sent to the treatment planning system (TPS). Based on these images the TPS would define positions and times for the radiation source to be placed. A dwell position for each catheter defines the exact location the radiation source will be positioned during the actual treatment and a dwell time defines the precise amount of time source will remain at that position. The TPS creates an optimal treatment plan made up of dwell positions for each catheter and dwell times for each position such that the radiation dose is delivered only to the area under treatment.

In Breast Brachytherapy, radiation is delivered by placing a High Dose Rate (HDR) Ir-192 source inside the body of the patient at precise locations in the tumor bed for precise amounts of time. The HDR source is located at the tip of a wire which is stored in a device known as the remote afterloader and the movement of the HDR source is controlled by a remote computer. Each catheter that is inserted in the patient is connected to one of the output channels of the afterloader by means of guided tubes. The plan generated by the TPS contains information regarding channel number, dwell positions and dwell time for each catheter. At the time of the actual treatment, the plan is sent to the remote computer controlling the afterloader. Thus during treatment, based on the treatment plan, the afterloader sends the HDR source to the programmed position through the appropriate output channel and keeps the HDR source at that position for the programmed time.

Quality Assurance (QA) procedures have been historically developed to minimize the likelihood of errors during High Dose Rate (HDR) treatment planning and delivery[9].

QA procedures have been designed for the treatment plan and separately also for the treatment delivery[9,10]. QA for the plan verifies the accuracy of the dose distribution by an independent calculation using information from the plan[11]. QA for the delivery verifies the spatial and temporal accuracy of the remotely driven radiation source. It also involves calibration of the source strength and calculating the total length of the applicator and transfer tube as well as verifying the correct connection of the transfer tube to the afterloader channel[9].

The above QA procedures have been developed to ensure correctness and accuracy of the treatment plan and treatment delivery. Yet non-verifiable assumptions still have to be made. For example it is assumed that there exists a similarity of anatomy and catheter position between planning and delivery instances. None of the current QA procedures guarantee accurate dose delivery or allow conformation of the actual source position. A small error in the plan or in the measurement of the transfer tubes or a faulty connection between the transfer tube and afterloader could accidently expose healthy tissue to unnecessary radiation which could cause irreversible damage to the tissue. A recent article in the New York Times spoke about such accidents during radiation treatments[12,13].

A breast brachytherapy treatment typically delivers a dose of 34Gy over ten fractions twice a day. So if an error occurs in the plan and is not detected in the first fraction it is very likely the same error will occur over all the 10 fractions. Although these accidents are very rare they do happen and steps have to be taken to avoid such mishaps in the future.

1.2 Objective of the Study

To date no commercial solution exists to track the actual source position during the delivery of the treatment and thus to reconstruct the actual dose delivered to the patient. This means that it is not possible to confirm the accurate delivery of the true treatment plan or check for the actual radiation dose received by the patient. The easiest solution one can think of is continuous imaging the HDR source using another radiation source during treatment. This cannot be used as the additional radiation source will add an unacceptable dose to the patient and the Nuclear Radiation Commission (NRC) prohibits the use of two radiation source at the same time.

This thesis details a proof of concept study of a novel QA method for brachytherapy treatments with the objective of reconstructing the position of the HDR source in 3D in real-time. This is done by simultaneously using the HDR radiation source for treatment as well as imaging purposes. The method utilizes the exit radiation of the HDR source to image a well defined matrix of markers and create projections which are captured using a flat panel detector (FPD). On processing the acquired image using morphological operations and noise cancellation filters, the coordinates of the projections are acquired while the coordinates of the markers are acquired through a calibration process (explained in chapter 3). The HDR source is considered as a point source. Thus the HDR source, the center of the marker and the projection of the marker would correspond to a line in 3D.

This method utilizes the above theory to calculate the source position by

calculating the intersection of two line defined by two different markers and its respective projections. The model calculates the point of intersection for all possible combinations of marker-projection pairs and uses the mean of all the calculated points to estimate the source position. This novel QA method would allow the user to quantify and record the *actual delivered dose distribution* as well as to monitor, compare and control in real-time the intended treatment vs. the delivered treatment.

The project involved designing the hardware model for the experiment set up and testing the design of the experiment; developing the software in MATLAB for reading and analyzing data and the software model for calculating the source position. The experiments were set up using test plans which sent the source to a pre-defined position and image data was acquired at each position. The image data was exported and then processed using the software to calculate the position of the source. The calculated source position was then compared to the planned dwell positions. From the results it is observed that the reconstructed dwell positions were within ±0.02cm of the planned dwell position.

CHAPTER 2 Background

2.1 Breast Cancer

Cancer is a disease found in humans characterized by the abnormal growth of cells which cannot be controlled[7]. Cancer cells are formed by defects to the genetic material of the cell. The defective gene can either be inherited or brought about by either damage to the DNA or introduction of new DNA due to a virus, exposure to radiation or chemicals, which destroy the genetic material of the cell causing mutations. The mutant cells do not die causing an abnormal population of cells to accumulate over time forming a tumor. A cancer cell originates in one part of the body and is named after that organ. Cancer cells can detach itself from the main tumor site and migrate to different parts of the body through the circulatory system or lymph vessels (metastasize)[7,14].

Breast cancer is a malignant cancer tumor that originates in the cells of the breast tissue mainly occurring in women[7]. It is the most common cancer found in women and the second leading cause of cancer related deaths in women[7,15]. The female breast is made up of the milk producing glands called lobules; tubes that connect the lobules to the nipples called ducts; fatty tissue around the lobules and ducts called the stroma; blood vessels and the lymphatic vessels (Figure 2)[16].

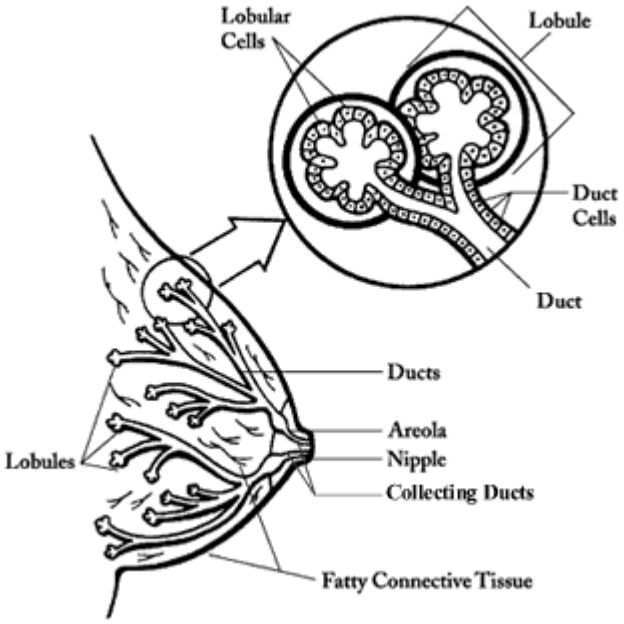

Figure 2: Structure of the female breast

Although the cause of breast cancer is still unknown, the cancer tumor is believed to originate in the cells that line the ducts or the cells that line the lobules in the breast. It is understood that the presence of the inherited BRCA1 and BRCA2 gene increases the chances of breast cancer in women[17]. Exposure to different risk factors such as radiation or chemicals can cause mutation of the gene leading to cancer cells.

Breast cancer can spread to different parts of the body by entering the lymphatic system. The cancer cells enter the lymphatic vessels and grow at the nodes in the chest, arm pits and areas near the collarbone. The cancer cells can also enter the blood stream and spread to other parts of the body[14].

2.2 Treatment of Breast Cancer

Breast cancer has been around for a very long time, dating back to the prehistoric era. The first case of cancer is assumed to be seen in Egypt found in the remains of mummies and also written about in ancient manuscripts[18]. The earliest record of breast cancer was found in Edwin Smith Surgical Papyrus, believed to be written in the Egyptian Pyramid Age[18]. The writings described this disease as not curable and the treatment then used was to burn the tumor or excise it using a knife[19]. This did not cure the disease as the tumor would reappear either at the same spot or at a different part of the body.

The renaissance ear witnessed advances in surgical procedures and a better understanding of the human anatomy through the introduction of autopsy. Andreas Vesalius described the anatomy of the breast which laid the foundation for future surgical methods for the treatment of breast cancer[20]. Till the 18th century various surgeons performed amputation of the breast as a treatment method. Surgery reached new heights with the discovery of anesthesia by Morton in 1846. This led to new developments in breast cancer surgery[19].

In the year 1882, William Stewart Halsted performed his first radical mastectomy, which involved surgically removing the tumor, underlying pectoral muscle, the axiliary lymph nodes and the surrounding tissue[18]. In 1894 Halsted published his work which was accepted by most surgeons in the late nineteenth century to become the standard for the treatment of breast cancer for the next one hundred years[19]. This method for treatment was called the Halsted radical mastectomy.

On the other hand Murphy and Grace opposed the radical mastectomy method of treatment[19]. In 1912, Murphy abandoned the Halsted operation. His method did not include the removing of the pectoral muscle. This approach marked the beginning of the modified radical mastectomy for breast cancer. Various clinical trials in the mid 1900's, proved this method to be as effective as radical mastectomy for early stage breast cancer[21].

The 20th century has witnessed a considerable evolution in breast cancer surgery. With the introduction of mammographic imaging screening and greater awareness amongst women, breast cancer could be detected at an earlier stage[2,22,23]. This prompted surgeons to advocate less radical operations. Attempts were carried out to preserve the part of the breast anatomy that did not contain the cancer. This led to the era of breast conservation surgery, which began in the mid twentieth century. It was known as lumpectomy or quadrantectomy and is defined by the excision of the tissue affected by cancer along with a portion of healthy tissue surrounding the tumor[22].

Although initial trials failed it was later realized that breast conservation followed by radiation therapy gave equally good results as compared with mastectomy through the landmark studies by Veronesi *et al*[24] in the 1970's and Fisher *et al*[25] in 1980's. Thus Breast conservation therapy replaced radical and modified mastectomy in the treatment of early stage breast cancer as it produced better cosmetic results and good local control. Lumpectomy followed by radiation till date remains the standard treatment for early breast cancer patients.

2.3 Radiation Therapy

The medical use of ionizing radiation in the treatment of cancer to control malignant tumors is known as Radiation Therapy (RT). One year after the groundbreaking discover of radioactive substance polonium and radium in 1898 by Marie Curie, Henri Becquerel reported the effects of radiation on normal human tissue[1]. This marked the beginning of radiobiology and radiation therapy. Radiation caused damage to the living tissue, permanently destroying the cells exposed to radiation[26]. This encouraged various physicians across the world to test radiation therapy for the treatment of cancer.

Breast cancer treatments has witnessed the use of radiation for over a hundred years with Gocht being the first to use radiation for the treatment of breast cancer as early as 1896, only a year after the discovery of X-rays by Roentgen in 1895[18]. Interstial radium therapy was introduced in 1903 for the treatment of cancer, where radium was inserted into the tissue of the malignant tumor. Janeway started using interstitial radium needles for the treatment of early breast cancer in 1915[27]. This marked the beginning of brachytherapy treatments for breast cancer.

In the 1920's, Geoffrey Keynes used radium needles without surgery to treat breast cancer. In his landmark publication in 1937, he reported results for ninety patients to be as good as radical mastectomy[28]. Despite these results radiation therapy was not widely practiced with radical and modified mastectomy predominantly the main method used for breast cancer treatment.

2.4 Breast Conservation Treatment Followed by RT

In the mid-twentieth century, many significant developments took place in the treatment of breast cancer, staring with mammography screenings. This led to the disease being detected at an early stage. Many medical centers all over the world implemented breast conservation surgery, which meant excision of only the tumor along with a nominal margin of healthy tissue surrounding the tumor. Advances in science led to new techniques to deliver radiation therapy with better accuracy. Machines using liner accelerators were readily available for external beam radiation therapy[23]. Brachytherapy with better dose delivery techniques were also available.

Randomized clinical trials of breast conservation surgery along with external beam radiation therapy to the entire breast were implemented[29]. Landmark studies of Veronesi *et al* and Fisher *et al* confirmed this new approach known as breast conservation therapy for the treatment of early stage breast cancer to be as effective as radical mastectomy[29].

Many patients may possess microscopic residual of the cancer after the conservation surgery with appropriate margins. Thus radiation therapy must be delivered to the entire breast and tumor cavity after breast conservation in order to irradiate the residue foci and obtain local control[26]. Interstitial brachytherapy was used as a boost dose in the 1970's[30,31]. External beam radiation therapy (EBRT) became readily available in the 1980's and this quickly replaced brachytherapy as the preferred boost method[31]. The obvious reason being EBRT was a non-invasive procedure which did not require additional surgery[30]. Other results showed EBRT alone with lumpectomy proved as effective as

mastectomy[32]. Despite this decline brachytherapy was still used as the boost technique for larger breasts with deep tumor site[30].

2.5 Accelerated Partial Breast Irradiation

When breast conservation therapy was implemented the radiation therapy that was adopted was whole breast irradiation as it was the most widely available technology and the easiest to apply. The success of this treatment approach has been recognized because of its results being equivalent to mastectomy with extended follow up[29,32]. In spite of this similarity many women eligible for breast conservation therapy do not choose this method of treatment[33]. One of the main reasons for this being the 6-7 weeks of post operative radiotherapy which requires everyday travel to the clinic[34]. This barrier forces a percentage of the women to either eliminate the radiation therapy procedure or choose mastectomy. Thus this approach for breast conservation therapy is not fully utilized[29].

A review of past breast conservation surgery with or without radiation therapy have recorded failure with reoccurrence of the tumor in the immediate vicinity of the lumpectomy cavity while other failures in the breast were found in only 1-3% of the patients[29,34,35]. This suggests that delivery of radiation treatment should be limited to the tumor bed rendering exposure of the remainder of the breast to radiation as insignificant. These findings have led to the utilization of partial breast irradiation[30,34].

In order to fully utilize the breast preservation techniques and reduce the overall treatment time, clinical trials were initiated using brachytherapy interstitial methods as the sole method for radiation therapy in breast conservation therapy[29,35]. Post operative radiotherapy was now reduced to 1-5 days "accelerated" as compared to 6-7 weeks and was being delivered only to the tumor bed "partial" as compared to the whole breast. This meant a change in treatment paradigm from whole breast irradiation to accelerated partial breast irradiation (APBI)[33]. A number of randomized clinical trials were carried out in order to support this change. Data from these pilot studies suggested that APBI treatments were successful when based on proper patient selection and surgical excision procedures followed by radiation therapy with appropriate dose delivery methods[29,33,36].

2.6 Breast Brachytherapy

Breast brachytherapy is a Radiation Therapy procedure typically delivered after lumpectomy as part of the breast conservation solution that was proven equivalent with mastectomy in selected patients. This procedure involves placing the radiation source either in the tumor cavity which means placing the radiation source inside the breast of the patient[37]. Breast brachytherapy has had a historical role to play in the radiation treatment of breast cancer[30]. Initially in the early 1900's it was used alone for the treatment of breast cancer. In 1929 Geofrey Kenynes was the first to publish results with brachytherapy used as the only method of treatment[28]. Although the results were impressive, brachytherapy has

been traditionally used as a boost for the treatment of early stage breast cancer and locally advanced breast cancer after mastectomy or BCS followed by whole breast irradiation[30].

The breast conservation era led to developments in the delivery method of brachytherapy treatments. During this time brachytherapy replaced the traditional mastectomy procedure for local recurrence after breast conservation surgery[38]. Major developments occurred in the past two decades with the introduction of accelerated partial breast irradiation. Brachytherapy played a historical role in the paradigm shift towards partial breast irradiation[33]. Improved multicatheter brachytherapy techniques and newer techniques such as the balloon catheter brachytherapy were made available with superior treatment planning mechanisms for dose delivery along with the introduction of remote after loaders[39]. These are the two most widely used modalities in the current era of brachytherapy treatments.

2.6.1 Multicatheter Interstitial Brachytherapy (MIB): This is the oldest technique used to deliver radiation therapy for breast cancer treatments dating back to the early nineteen hundreds. MIB was used to deliver a boost dose following whole breast irradiation in the 1970's. It became popular in the 1990's with all initial trials for APBI being performed using MIB[29,35,36]. In the past decade this method has been used for the treatment of early stage breast cancer by delivering radiation only to the part of the breast tissue which is at greatest risk for the tumor to reoccur[35,36]. This is done by placing catheters through the breast tissue surrounding the tumor cavity (Figure 1)[8,39]. The catheters are usually inserted at the time of lumpectomy surgery or a few days later. This technique would require 14 -

20 catheters, depending on the size of the tumor[35]. In order to avoid hot-cold spots, catheters are placed at intervals of 1.5cm from each other[33,35]. The catheters are inserted either using the free-hand approach or template approach. Image guided techniques can be used in either approach with the help of ultrasound or CT[8,40]. The configuration of the catheters with respect to the tumor is very important for effective and homogenous dose delivery[41]. Once the catheters are in the desired position, a complete computed-tomography (CT) data set is acquired and used to outline the tumor and catheter geometry[40]. Treatment planning software (BrachyVision) is used to compute the plan for dwell positions and dwell times in order to deliver the prescribed dose to the tumor bed with a well defined margin of surrounding tissue[36,40,41]. The catheters are then remotely after-loaded according to the treatment plan with a high-does-rate radioactive source[40].

2.6.2 MammoSite Balloon Brachytherapy: Although the local control produced by the multicatheter technique was excellent, the technique required expert training and thus was not offered at all institutions across the US[42]. The cosmetic was not satisfactory because of the scars left at the catheter incision site[42]. This led researchers to investigate a less invasive treatment approach[43]. The MammoSite Radiation therapy System was developed by Cytyc Inc. to simplify the brachytherapy treatment procedure and improve patient comfort[33,42].

The MammoSite device is made up of a silicon balloon attached to one end of a double lumen catheter[42,43]. The device is placed in the lumpectomy cavity either during the breast conservation surgery or a few days later. The catheter contains two channels, one for

inflation of the balloon and the other to deliver the HDR radiation source. A saline solution is used to inflate the balloon such that it occupies the entire lumpectomy cavity. Small amounts of contrast material are mixed with the saline solution for radiographic visualization.

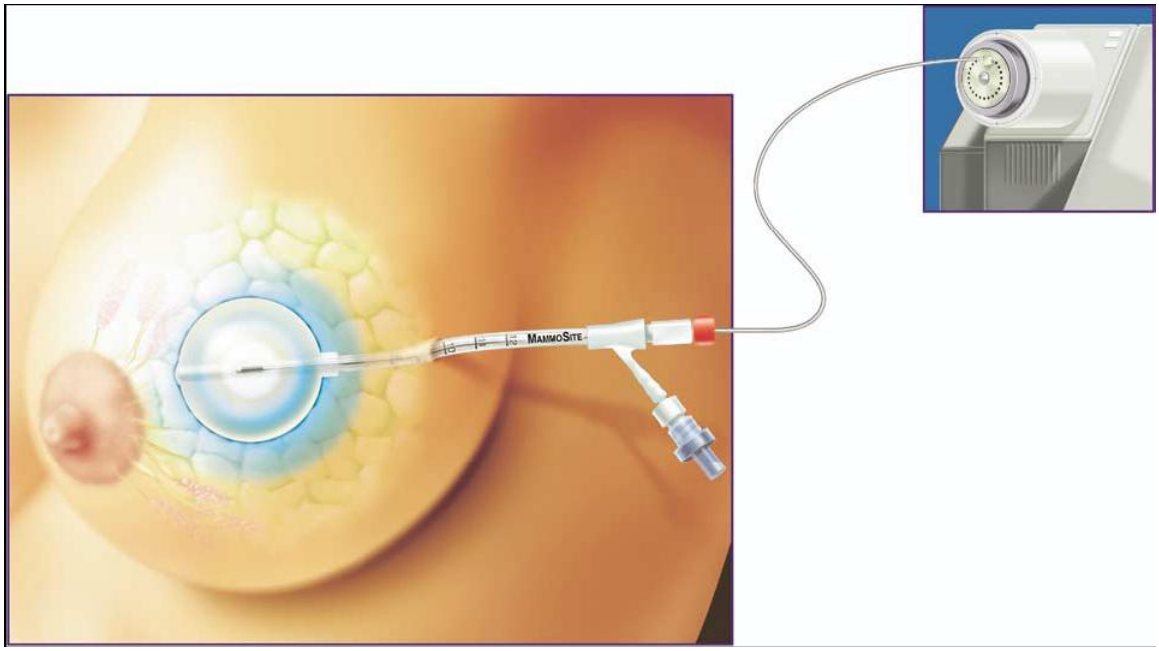

Figure 3: MammoSite balloon brachytherapy[37]

Once the device is surgically placed in the lumpectomy cavity a complete CT image data set is acquired to review the quality of the implant and for radiation treatment planning. The quality of the implant is based on two important variables: balloon to skin distance (minimum 5mm) and symmetry of the balloon with respect to the catheter. The treatment plan is created such that radiation is delivered to the tissue immediately surrounding the lumpectomy cavity. The device is then remotely after-loaded according to the treatment plan with a high-does-rate radioactive source.

2.7 Remote Afterloader

Remote afterloader is a treatment delivery unit which holds a single cable that contains the radiation source at its tip. A remote operating console drives the cable containing the source such that it steps to each position in the catheter as programmed by the treatment planning system and keeps it there for a precise amount of time.

Figure 4: VariSource remote afterloader (Varian Medical Inc.)

Figure 4 shows the VariSource afterloader (Varian Medical Inc.). Transfer tubes are used to connect the output channels of the afterloader to the catheters in the patients. During treatment the cable with the source travels through one of the output channels to a

catheter in the patient via the transfer tube. Once a given catheter has been treated the source is retracted into the afterloader and transmitted into the next catheter for treatment.

2.8 High Dose Rate Radiation Source

Iridium-192 is the most common High Dose Rate (HDR) radiation used in remote afterloaders[31,44]. The Ir-192 source is located at the tip of a wire which is stored in the afterloader.

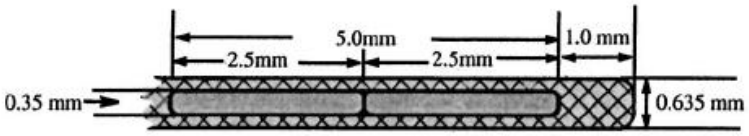

Figure 5: Ir-192 source by Varian Medical Systems Inc

Ir-192 has a low average energy and thus can be easily shielded by 0.3cm of lead. Ir-192 possesses high specific activity and thus allows the construction of high activity source (10Ci) with a relatively small diameter. Figure 5 depicts the Ir-192 source for the VariSource afterloader. It is 5mm in length with a diameter of 0.35mm. The half life for Ir-192 is approximately 74 days. A typical source strength during treatment ranges from 10Ci to 3Ci. Thus the Ir-192 source has to be changed once every 3 – 4 months.

2.9 Radiation Treatment Planning Workflow

2.9.1 Catheter Implantation: For both techniques the catheters are implanted either during the lumpectomy surgery or a few days later. Catheters are placed using CT-guided 3D planning software such as Pinnacle Planning Software (Philips Medical Systems)[40,41]. A pre-planning CT scan is obtained to locate the tumor cavity[40]. Based on these scans the software outlines the cavity and creates a design for the catheter placement which includes catheter number, catheter planes, intercatheter spacing and direction of placement[40,41] (Figure 6).

Figure 6: Tumor outline and planning for catheter placement

Using this design the entry-exit points for the catheters are marked on the skin of the patient. 2-3 trocars are inserted in the marked points followed by a CT scan to evaluate the position of the trocar and the tumor cavity. Based on this information the remaining

trocars are inserted and a CT scan is acquired to evaluate the accuracy of the trocar placement[41]. Once the trocars are precisely placed, they are replaced by the afterloading catheters and tightly secured by buttons at both ends[40,41]. For quality assurance purposes the different color buttons are used for different planes. The catheters are then numbered and length of each catheter is recorded[11] (Figure 7). This completes the catheter implantation procedure for the multicatheter interstitial technique.

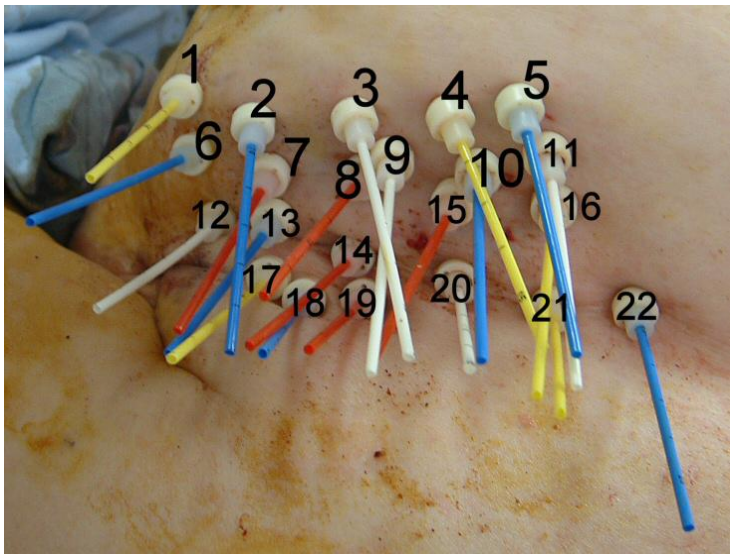

Figure 7: Multicatheter implants for APBI treatments

The Mammosite device is implanted using an open technique (during the lumpectomy surgery) or using ultrasound techniques to estimate the tumor cavity (post-lumpectomy). Once the device is in place CT scans are used to evaluate the quality of the implant.

2.9.2 Treatment Planning: CT scans are acquired to compile an image dataset of the tumor bed and catheters by inserting dummy wires in the inserted catheters[40]. This image data set is used for the 3D dosimetric planning of the HDR treatment[41]. The dataset is electronically transferred to the treatment planning station (Brachyvision Planning System, Varian Inc.)[8,41]. First the lumpectomy cavity is contoured along with other anatomical structures[11]. Treatment planning tools are used to expand the cavity by 1-2cm, keeping a 5mm distance from the chest wall, pectoral muscle and the skin surface[11,40,41]. The expansion depends on the size of the breast and the lumpectomy cavities size and location. This new volume is called the planning target volume.

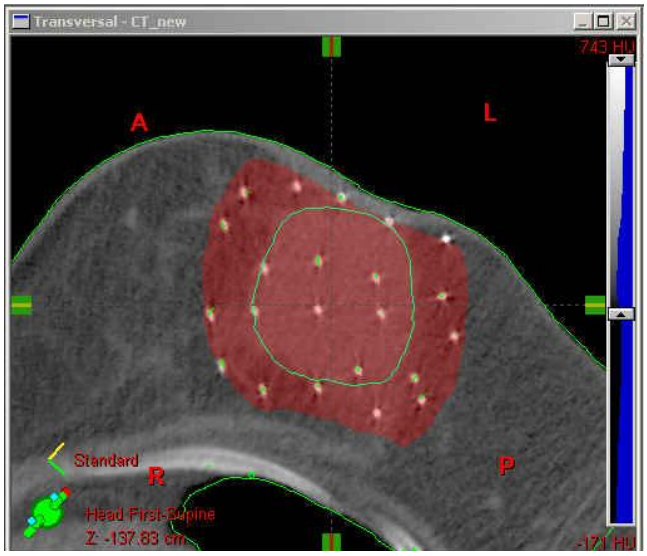

Figure 8: Contouring of tumor cavity and target volumes

Next the applicators are outlined using the 3D planning software and the CT images. The catheters are reconstructed along the dummy wire from one end of the catheter to the other. Each catheter is numbered and defined by several dwell positions.

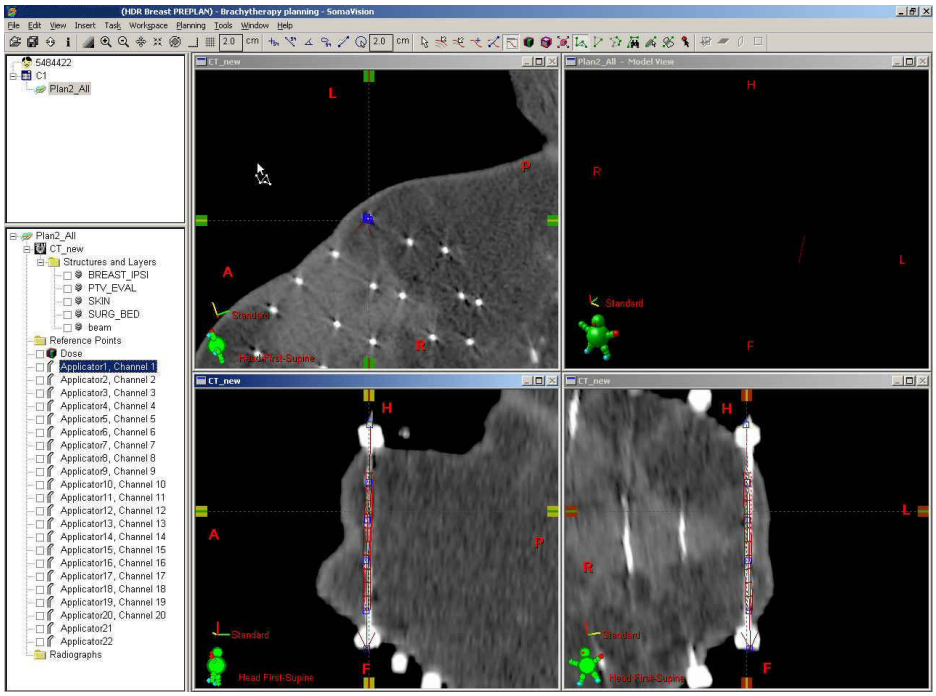

Figure 9: Explaining outlining of applicator and definition of dwell positions

The planning system creates a treatment plan by defining dwell times for each dwell position for all catheters target volumes. The aim of the plan is to delivery 100% of the prescribed dose to the target volume. Dose optimization is performed using the geometry based method and the Dose-Volume Histogram method.

Dose Homogeneity Index (DHI) is used to measure the dose homogeneity of the implant and for a good implant should be as high as possible[11]. DHI is defined as,

$$DHI = (V100 - V150)/V100$$

where V100 is the absolute volume of tissue receiving 100% of the prescribed dose and V150 is volume receiving 150% for the prescribed dose. The treatment plan is then evaluated using Dose-Volume Histograms. Similar procedure is followed for the planning of a MammoSite treatment delivery.

The treatment plan is then exported into the computer controlling the afterloading machine. A treatment plan is made up of dwell times and dwell positions for each applicator. The catheter lengths are added to the appropriate applicator and fed to the treatment delivery system. Patients are treated with a prescribed dose of 34Gy delivered in 10 fractions over 5 days (two fractions a day at 6 hour intervals).

2.9.3 Quality Assurance (QA) Procedures: QA procedures are carried out for the treatment plan as well as the treatment delivery. QA for the plan involves verifying the accuracy of the optimized dose distribution created by the treatment planning system. Typically this implies a simple independent calculation of either point dose approximation or volume based calculations using information from the plan such as total time and source strength and comparing it with the equivalent point on the treatment planning system. QA for the plan is performed and approved by a physicist other than the one who created the plan.

QA for the delivery verifies the spatial and temporal accuracy of the remotely driven radiation source[9,10]. It also involves calibration of the source strength and calculating the total length of the applicator and transfer tube as well as verifying the correct connection of the transfer tube to the afterloader channel[9]. Figure 10[45] depicts a QA chart for the delivery which includes source activity, source positioning accuracy and time accuracy. The total length of the source transfer tube along with its corresponding catheter is calculated for each catheter. This number is then added to the dwell positions for each

output channels of the afterloader. Finally during actual treatment delivery the treatment plan is checked against the treatment delivery print out generated by the afterloader.

HDR FULL CALIBRATION

Date: December 5,2005 Time: 10:20

1. SOURCE ACTIVITY

Chamber: Standard Imaging HDR 1000 Plus; S/N A943623
Electrometer: CNMC K602; S/N 51090

Source #	Stated activity	Reference date	Check date	Decayed act
D35A-2870	41250	11/17/2005	12/5/2005	34852.6471

T =	23.2	C t,p:	1.0188	
P =	749	Calibration factor:	4921	Calibrated: Apr 05
		Electrometer factor:	0.981	Calibrated: Oct 04

Position	Electr. rdgs Rdg (Amp E-08)
940	7.066
945	7.102
950	7.117
955	7.109
960	7.077

Measured activity (U) 35003.72 8.68 Ci
Ratio: measured/stated activity 1.0043

____ within ± 5%

2. SOURCE POSITIONING ACCURACY (Mode 13)

Programmed Distance (mm)	Measured Distance (mm)	Actual Distance (-2.15mm)	Deviation (mm)
905	907.5	905.35	0.35
995	997	994.85	-0.15

____ within 1 mm

3. BATTERY BACK-UP

____ Source retracted from treatment position when power to the unit was interrupted

____ Printout indicated failure due to power interruption and gave source out time and position

4. LENGTH OF SOURCE TRANSFER TUBES & APPLICATO (changes < 1 mm)

____ transfer tubes for flexible applicators ____ transfer tubes for rigid applicators

____ transfer tubes for gyn applicators ____ applicators

5. TIMER ACCURACY & LINEARITY d = 950mm

Time (s)	Q x 10⁻²	Slope = ΔQ/ΔT	Timer Error = (Q2-2Q1)ΔT/(Q2-Q1)
5	3.755		
10	7.176	0.6842	-0.4882
20	14.005	0.683	-0.5066

____ timer error < 1 s

Figure 10: QA chart for treatment delivery

CHAPTER 3 Methods and Materials

The experiment for this study was setup in the state-of-the-art brachytherapy imaging suite located in the basement of the North Hospital at VCU Massey Cancer Center. The tracking of the HDR source requires three basic elements; an imaging source, an array of markers and a detector. X-rays from the Brachytherapy simulation machine (Acuity, Varian Inc.) was used as the imaging source for calibration purposes while the HDR source was used for all other imaging purposes. The flat panel detector was used as the detector for all the test runs. Ball bearings (BB's) of 4mm to 6mm in diameter purchased from Pleasants Hardware and a local bicycle shop were used as markers.

A basic experimental setup for the study would be to position the HDR source at some distance away from the detector and place a set of markers at some distance between the source and the detector. Figure 11 illustrates the schematic representation of the experiment for the tracking the HDR source. The figure depicts two planes namely the detector plane and the marker plane. The surface of the flat panel detector makes up the detector plane while the top surface of the plexiglass makes up the marker plane. Let's assume P1 and P2 represent two markers placed at some random position on the plexiglass. The system of axis was chosen such that center of the detector acts as the origin, the x-axis and y-axis run through the center of the detector and the z-axis is perpendicular to the

center of the detector. This system of axis was chosen as it was convenient and made calculations easier. For all our experiments we used a single test applicator placed along the x-axis.

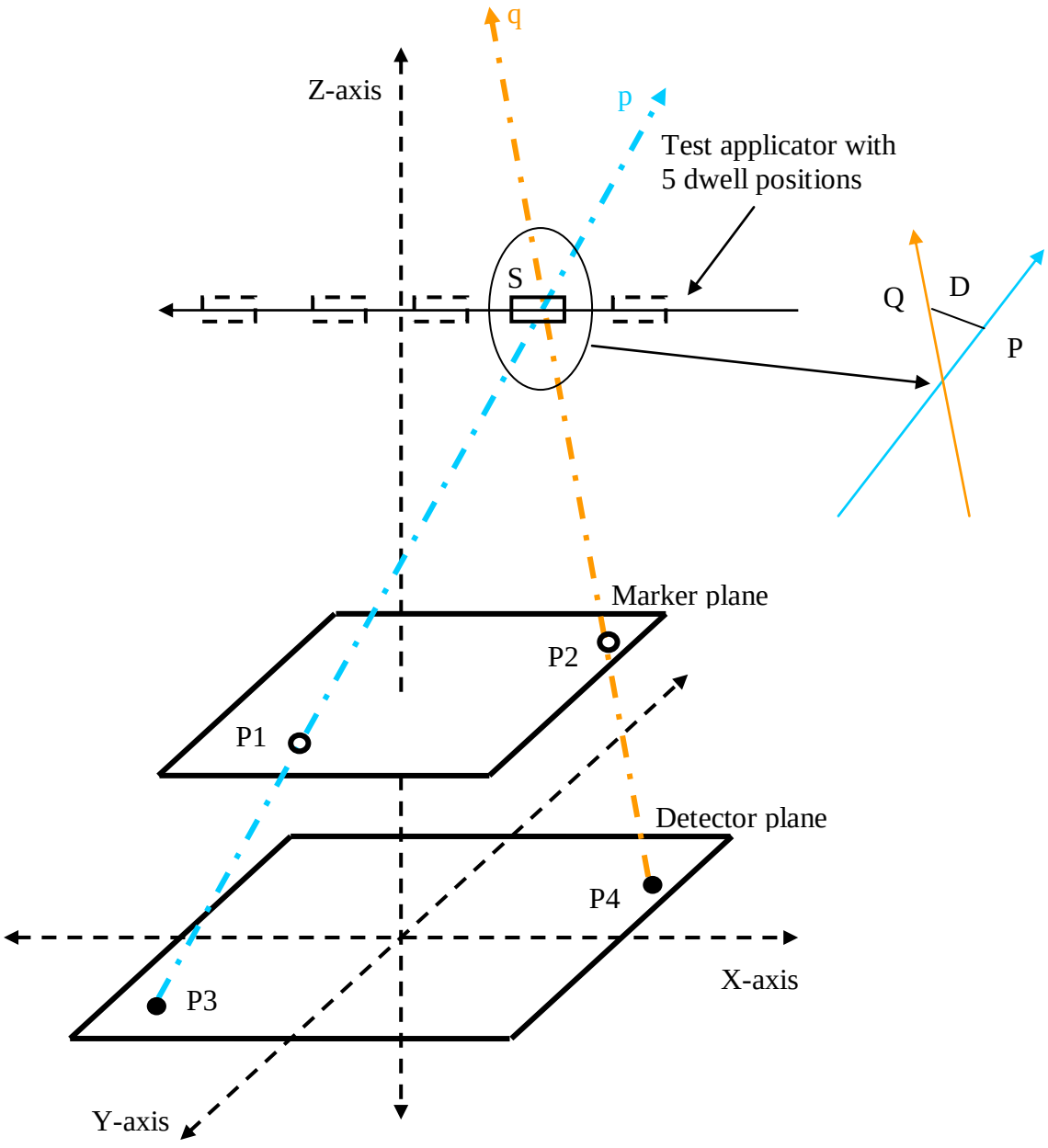

Figure 11: Explaining the schematic of the experiment

Now let's assume point S is one of the dwell positions where the HDR source will be active for a certain amount of time. When the HDR source reaches point S and is active, it will produce projections of the markers on the detector. Thus, marker P1 will produce projection P3 on the detector while marker P2 will produce projection P4 on the detector.

Once the coordinates of the markers and its projections with respect to the origin are known in space, we can define a line in 3-D which passes through the marker and its projection. Line p is defined by the combination of marker P1 and its projection P3 while line q is defined by the combination of marker P2 and its projection P4. The intersection of these two imaginary lines p and q in 3-D space will give the original position of the source S. The same procedure is repeated to track all other dwell positions.

It is not necessary for two non parallel lines to intersect in space. Most non parallel lines do not have any points in common. They go over or under the other without touching. Thus to plot the true intersection of line p and line q in space is very unlikely. Instead we compute the shortest distance between the two lines. When two lines in 3-D do not intersect they can be connected by a line segment which is perpendicular to both the lines. The shortest such line segment is unique and is considered to be the true intersection of the two lines in 3-D. The shortest distance between line p and line q is represented by D, while P and Q represent the corresponding two points contained on line p and line that make up D. The mean of the coordinates of point P and point Q would give us the 3-D coordinates of the source position.

The above schematic represents only two markers. From the above explanation it is confirmed that a single pair of markers and their projections are required to calculate the source position. For this study a well defined matrix of markers is used. The above procedure is repeated for all possible combination of marker – projection pairs. N markers, would produce N * (N-1) / 2 combinations of marker – projection pairs, each pair producing a shortest distance D, a P and a Q. The average over all the P's and Q's will give the most accurate position of the source.

3.1 Testing Imaging Geometry and Image Quality

Initially it has to be known if the radiation produced by the HDR source is strong enough to be used as an imaging source. The flat panel detector (FPD) of the imagining machine (Acuity, Varian Inc.) is optimized for the low energy of the imaging X-ray source (80 - 120 kV range). The average energy of Ir-192 source used for HDR treatments is approximately 380keV, well outside of the range for which the FPD is optimized. Given the likely large distance (0.5-1.0m) from the treatment radioactive Ir-192 source to the FPD, the intensity of the 'beam' is going to be significantly less than of the X-ray source, which will translate in low S/N ratios.

The aim of this test is to define the best imaging geometry for the experiment: the best possible design of markers, optimal position of the source and the detector; and to test image quality: to check if the projections of the markers produced by the HDR source for different source – detector distance can be isolated and labeled.

A good imaging geometry would include a well defined matrix of markers and an optimal height between the markers and the detector, such that every marker of the matrix produces a projection on the detector. The issue of optimal height is really finding the best compromise between large image displacement and good image quality. Let's assume the source moves from position S1 to position S2 (figure 12). When the markers are placed away from the source and closer to the detector the resulting scatter will be significantly less, thus producing good quality images. But the displacement of the markers projection on the flat panel detector for a given source displacement would be very small relative to the detectors resolution that is 0.388mm. When the markers are placed closer to the source and away from the detector, although the displacement of the projection of the markers would be larger, larger amounts of scatter would deteriorate the quality of the image.

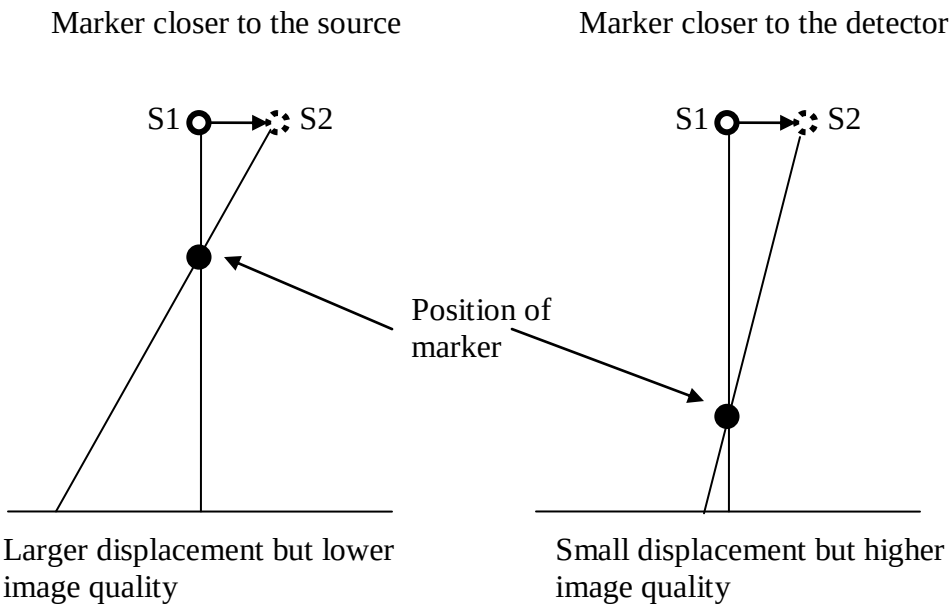

Figure 12: Explaining position of the markers for a good imaging geometry

An average breast cancer tumor is less than 15cm x 10cm x 10cm cube. Thus for the calculations we assumed that the source would travel a maximum of 15cm in the x-axis and 10cm in the y-axis within the tumor. The dimension of the detector is 40cm x 30cm. A region has to be defined such that when the matrix of markers is placed within that region, every single marker in the matrix would produce a projection on the detector.

The source-detector distance is assumed to be 60cm. Let's assume line AB represents the 15cm side of the cube that the source is supposed to travel within the tumor and line PQ represents one side of the detector (figure 13).

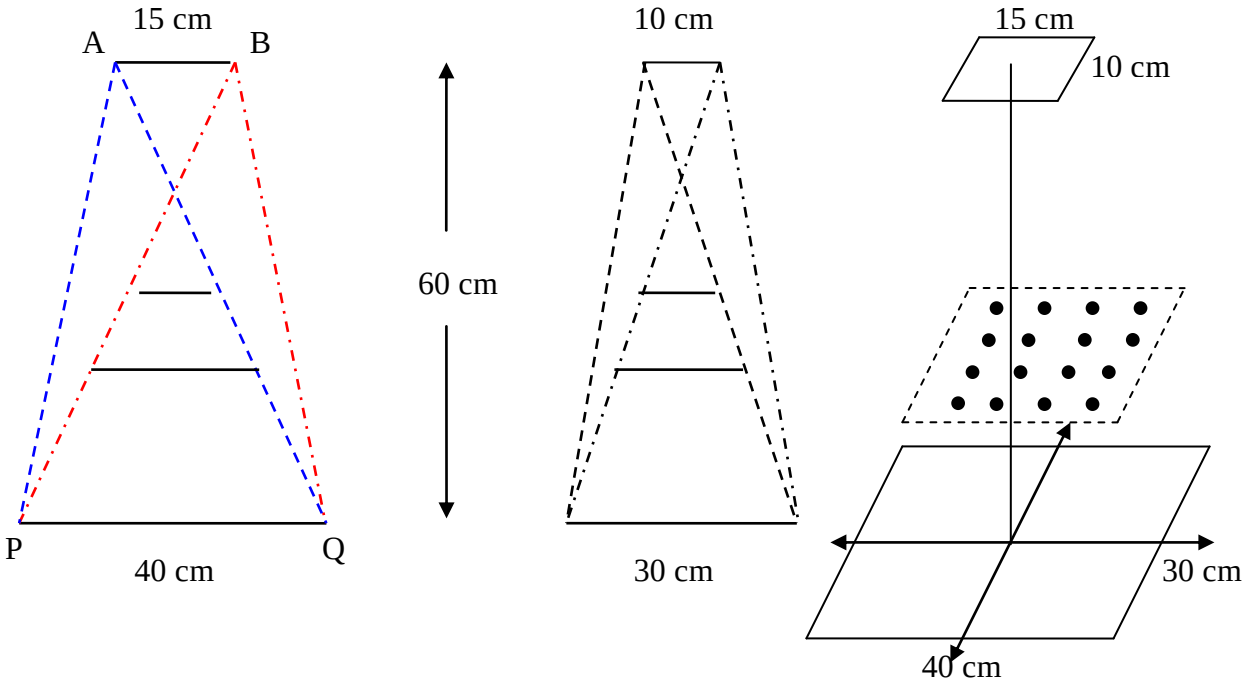

Figure 13: Explaining the area of interest for the position of the markers

When the source is at point A, all markers within the area covered by the blue dotted lines will produce projections on the detector. Now when the source is at point B all

markers within the area covered by the red dotted lines will produce projections on the detector. The intersection of these two areas defines our area of interest. Within this area we need to find the optimal height such that there is no compromise on image quality and distance of image displacement at the same time there is room for a decent amount of markers to be produced on the detector. From the figure above it is realized that 20cm – 30cm is a good height to place a well defined set of markers such that all the projections fall on the detector.

Once the range of distances between the marker and the detector has been defined, the basic experiment is set up by placing the plexiglass mount on top of the cover of the detector and acquire images using the HDR source. Markers with different diameters were placed 1cm and 2cm apart on top of the plexiglass surface. The markers were placed along the two central axis of the detector. The source - detector distance was varied from 40cm – 70cm with an increment of 5cm, keeping the distance between the markers and the detector constant at approximately 20cm. Images were acquired using the HDR source and the flat panel detector.

In order to use the combination of the HDR source along with the detector, the x-ray source has to be eliminated in some way or the other. This is achieved by closing the doors of the x-ray beam. By doing this the only radiation source available for imaging is the HDR source. The activity of the HDR source will produce projections of the markers on the flat panel detector and these can be captured on the detector by the push of a button in the control area. Images are then named and saved in the hard drive memory of the remote computer which operates the Acuity machine in a specified folder. From here these

raw images are exported onto an external computer in the DICOM format and processed using MATLAB.

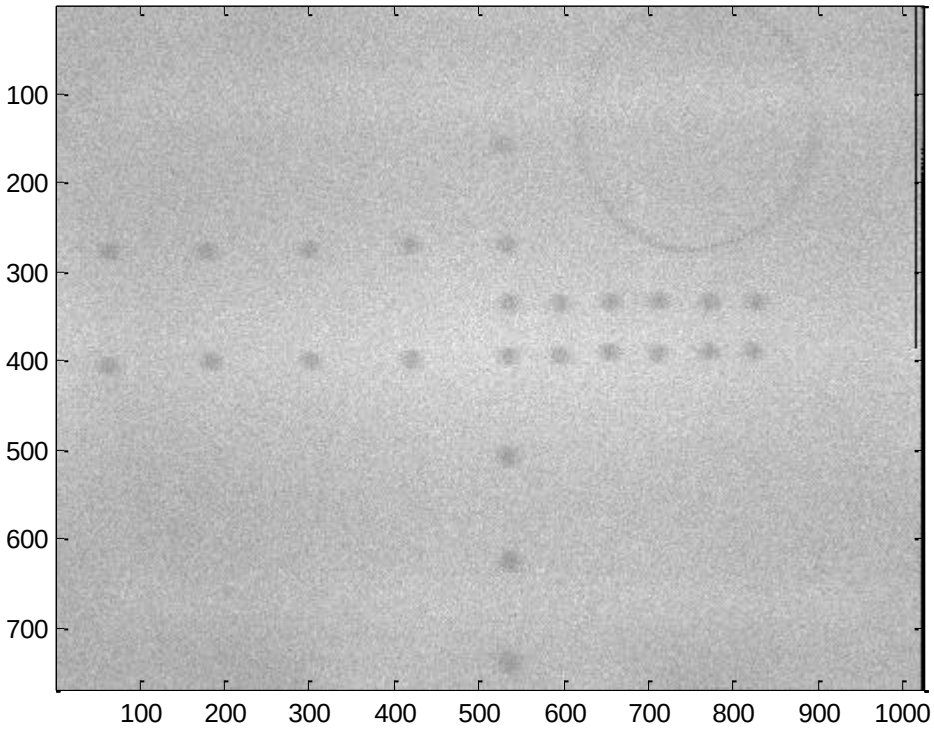

Figure 14: Grey scale image acquired using the HDR source and flat panel detector with source – detector distance 50cm to test imaging geometry and quality

Figure 14 depicts a grey scale image of the projection of markers when the source – detector distance was 50cm. The initial set of images which were taken to check image quality proved that the markers could easily be seen by the naked eye. The best quality images were produced when the source – detector distance was at 50cm and when the markers were spaced 2cm apart.

The next step was to segment out only the markers, label them and get their centroids. The centroid would be used as a surrogate for the coordinates for the projection

of the markers. The raw images were saved in the DICOM format and could be read in MATLAB by using the Dicomread command as explained below.

```
info = dicominfo(FileName);
X = dicomread(info);
```

"dicominfo" reads the metadata from the DICOM file specified by the string FileName and stores it in the variable info. "dicomread" reads the image data from the DICOM metadata structure 'info'.

The image data consists of the projection of the markers and random noise. Image averaging and noise filters were used to remove the noise. Once a smoother gray scale image with minor grains is obtained, the aim was to segment out only the markers and leave out the noise. The shape of the markers is known before hand, thus morphological operations were used to localize and segment the markers. A threshold is applied to convert the gray scale image to a binary image in which the markers are represented by ones and the rest by zeros (image processing explained later in the chapter). Thus from the binary image the markers could be easily segmented, labeled and their centroids could be calculated.

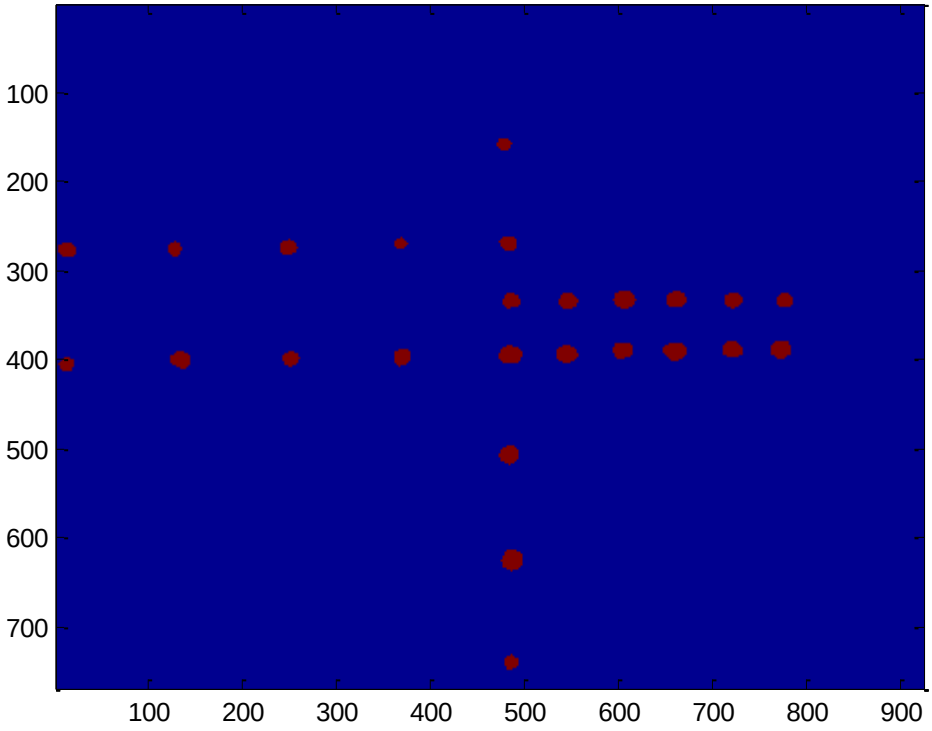

Figure 15: Binary image obtained after morphologically processing and segmenting the grey scale image

3.2 Experimental Setup

The brachytherapy imaging suite at Virginia Commonwealth University is equipped with Acuity which is an imaging and simulation machine manufactured by Varian Medical System, Inc. The Acuity machine is equipped with a C-arm gantry system, where the x-ray source makes up one end of the C-arm and the flat panel detector makes up the other end. Of all the equipment present in the suite the Acuity imaging machine, the

flat panel detector, the afterloader, guide tubes, a 5cm solid water phantom, test catheter and the operating couch were used for the experiment.

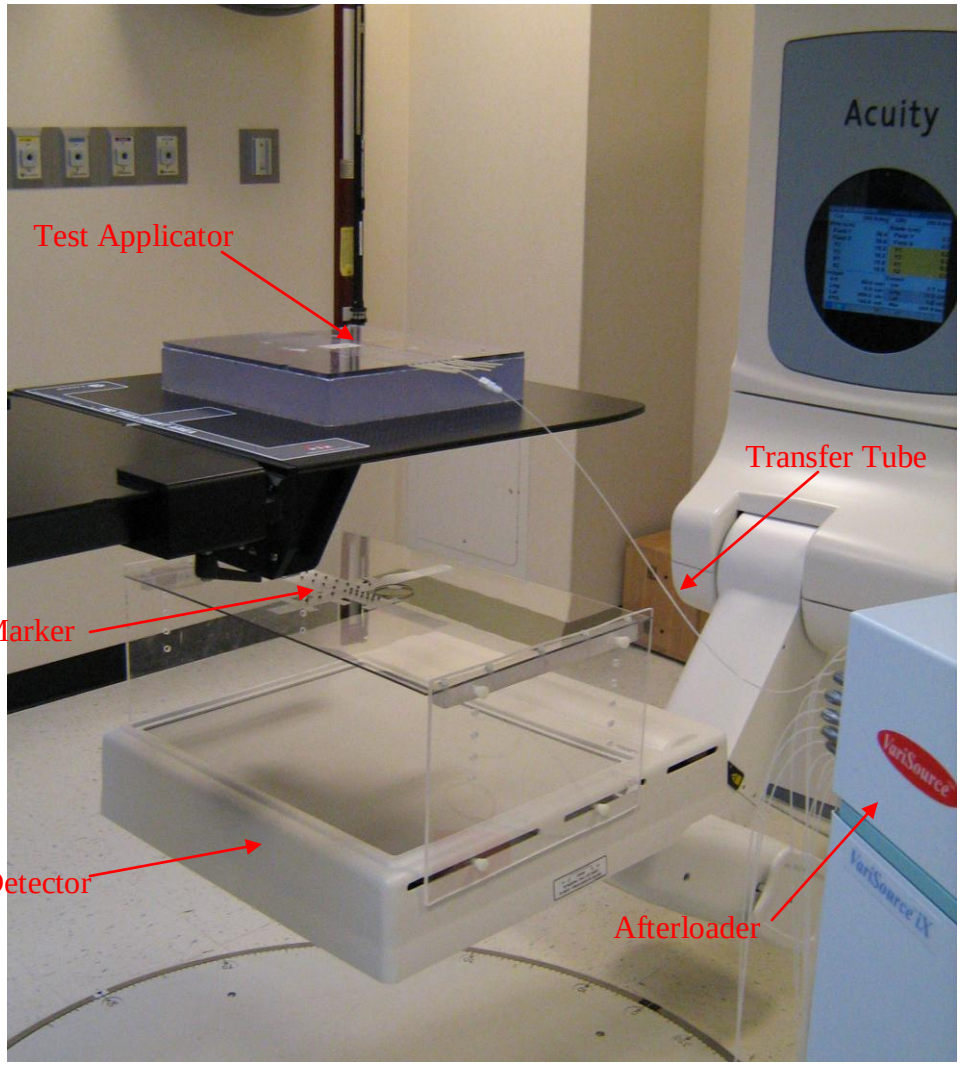

Figure 16: Representation of the experimental setup

The flat panel detector of the Acuity machine was used as the detector for all experimental purposes. The flat panel detector is a PaxScan 4030CB, amorphous silicon digital x-ray detector, manufactured by Varian Medical System Inc. The total pixel area of

the detector is approximately 40cm (h) x 30cm (v), with a total pixel matrix of 1024 (h) x 768 (v) at half resolution and 2048 (h) x 1536 (v) at full resolution. For all the experiments the detector was used at half resolution with a pixel size of 0.0388cm. The flat panel detector is placed inside a white plastic cover, to help protect it from the external environment. The detector can be programmed to move in any direction giving us the liberty to place it wherever we please.

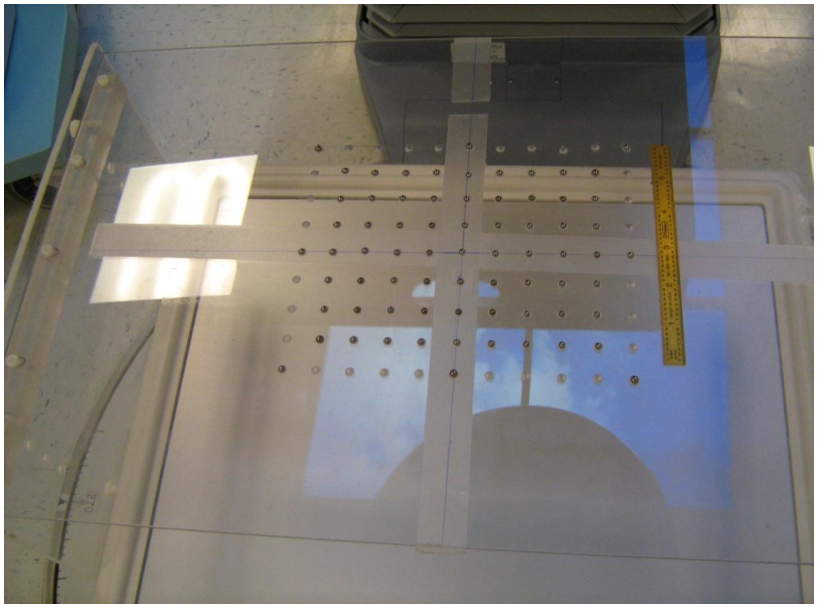

Figure 17: Representing the arrangement of well defined matrix of markers

In order to hold the markers at a fixed height above the detector an in-house mount was made out of plexiglass. This plexiglass arrangement could be mounted on top of the cover of the flat panel detector with the help of screws. The height of the mount could also

be varied with the help of adjustable screws. The markers were arranged in the form of a well defined matrix. Figure 17 shows a well defined arrangement of the markers.

The HDR source used was the iridium 192. The HDR source was stored and delivered using the afterloader present in the suite. The afterloader used was VariSource iX (Varian Medical System, Inc.). The HDR source is present at one of the ends of the source wire which is stored in the afterloader in a highly shielded environment. The afterloader is controlled by a remote operating console which uses a source control and drive mechanism to sort, control and move the source into specific positions for specific amounts of time. The VariSource iX has twenty output channels, with guided tubes connected to each output. The HDR source can be programmed to be delivered through any of the twenty output channels. Guided tubes are long rubber catheters which connect one of the output channels of the afterloader to the test catheter.

The test catheter used for the experiment is a 0.6 cm thick sheet of plexiglass. The plexiglass sheet contained horizontal cylindrical holes of 0.5 cm in diameter which were sealed from one side and open from the other. The test catheter was placed inside these holes with some part of the catheter left outside the plexiglass. The guided tubes were clipped on to the part of the catheter left outside the plexiglass, thus connecting the afterloader to the test catheter.

A 5cm solid water phantom was used to mimic the patient. The test catheter was placed on top of the solid water and this arrangement was placed on the operating couch to portray an actual treatment scenario. The afterloader delivers the HDR source through the

guided tubes to a particular position in the test catheter and holds the source in that position for a particular amount of time.

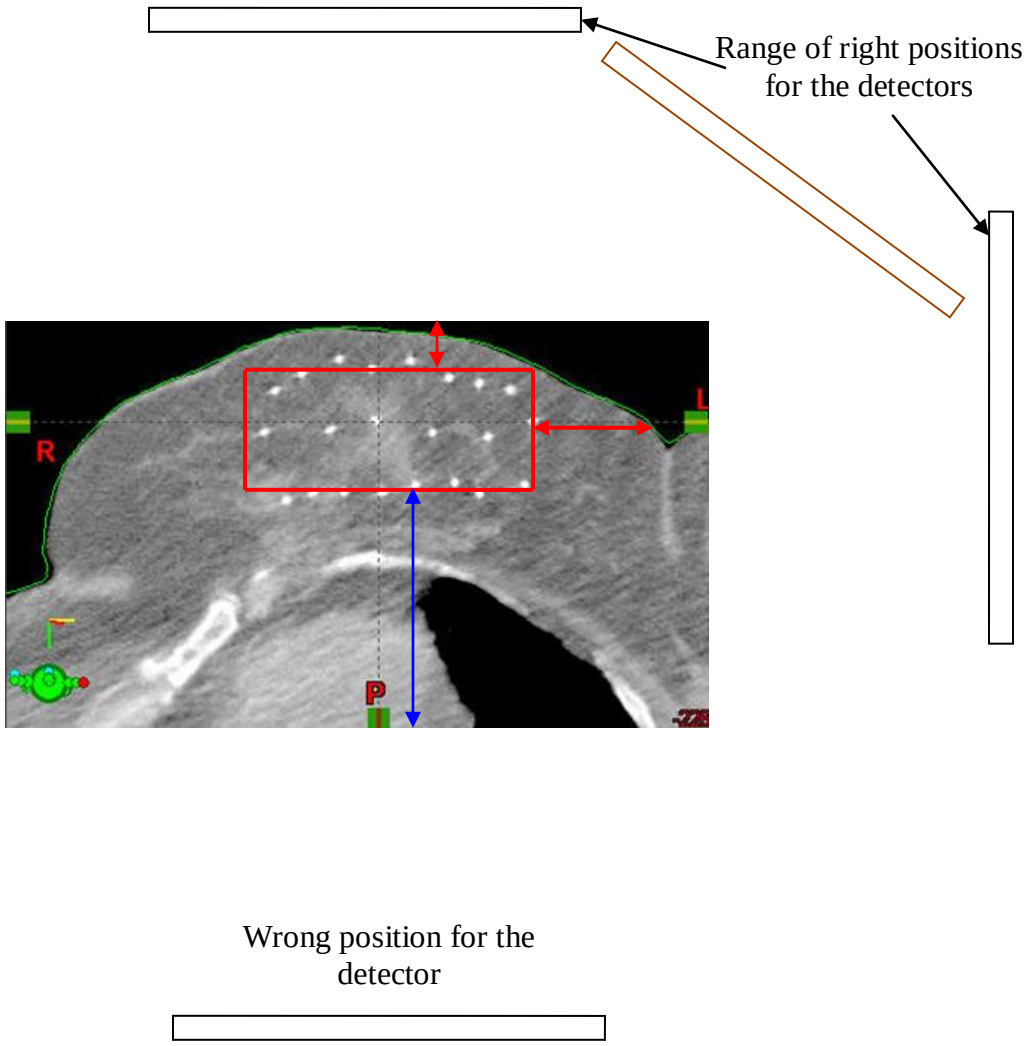

Figure 18: Explaining the correct positioning of the flat panel detector

For the experimental setup of the study, the detector is placed below the operating couch only for convenience. The flat panel detector is attached at one end of the C-arm of the acuity machine and can be moved in all directions. If this set up was to be used for a

real patient, the attenuation caused by the body of the patient (blue arrow in figure 18) would be very large, thus affecting the quality of the image. The solution would be to place the detector in such a position suck that the attenuation caused by the body of the patient would be kept to the minimum. One way is to either place the detector directly above the patient or perpendicular to the patient, depending on the location of the tumor. This gives a rage of positions to place the detector with the ideal position would be to place the detector at a 45 degree angle (shown in orange in figure18). For such an arrangement we assume the maximum distance the radiation would travel within the body of the patient would not be greater than 5cm (red arrows in figure 18). This is why a 5cm solid water phantom is used to mimic the patient for all the experiments.

3.3 Calibrating the System

Calibrating the system is a twofold process. The first is to calculate the exact height between the marker plane and the detector plane while the second is to calculate the coordinates of the position of the markers with respect to the origin. The actual surface of the detector is hidden inside the cover of the flat panel detector. So the height between the markers and detector cannot be manually measured. The plexiglass mount used to place the markers is not stable. It is a temporary arrangement and has to be dismantled and reassembled every time the experiment is executed. This will lead to a change in the

position of the markers every time the experiment is executed. Thus it is very important to calibrate the system before performing any other calculations. For both the calibration procedures images were acquire using the x-ray source which is kept at a known height.

3.3.1 Calculate Height: The temporary and unstable nature of the plexiglass mount adds to the uncertainties in the height between the marker plane and the detector plane. In order to calculate the coordinates of the markers on the marker plane the exact height between the two planes has to be known. Figure below represents the image acquired using the x-ray source.

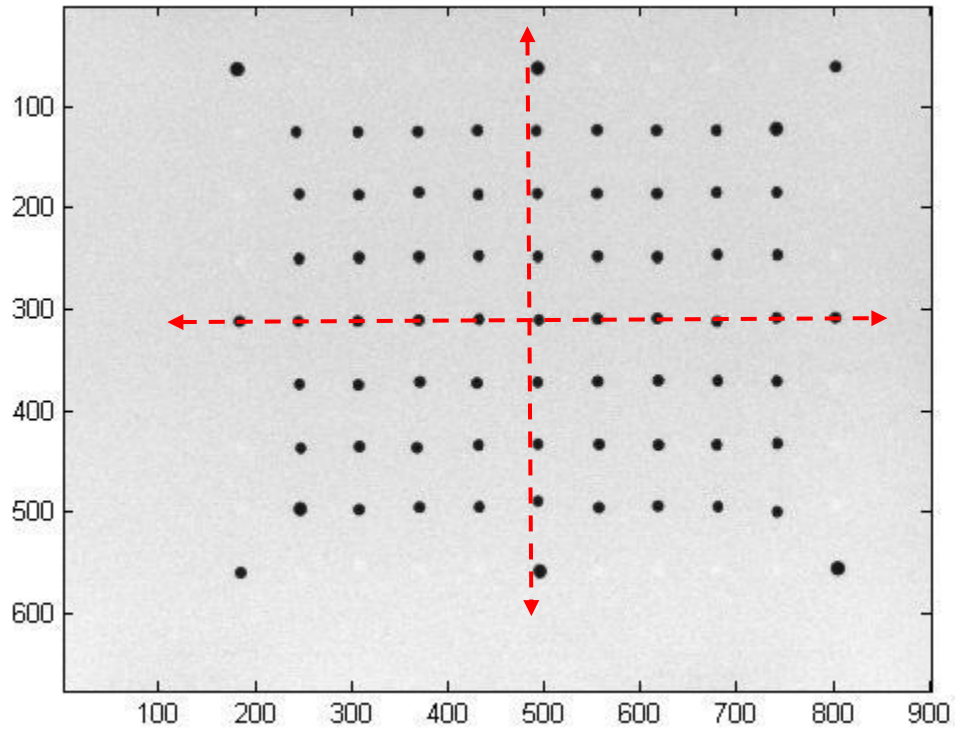

Figure 19: Grey scale calibration image, red dotted lined representing the central axes

The markers are arranged such that there exists an array of markers along the x-axis and y-axis. These markers along the central axis are used to calculate the height between the two planes. From figure 19 a marker exists on the axis of the origin. Using this marker as a reference, distances to other markers along the x-axis and y-axis are calculated for the projections and the markers. In order to get the distance between the projections of the markers, the raw image is morphologically processed so that it can be segmented and labeled, and the centroid of the projections of the markers is calculated. Using these distance we can calculate the height H using the formulae below.

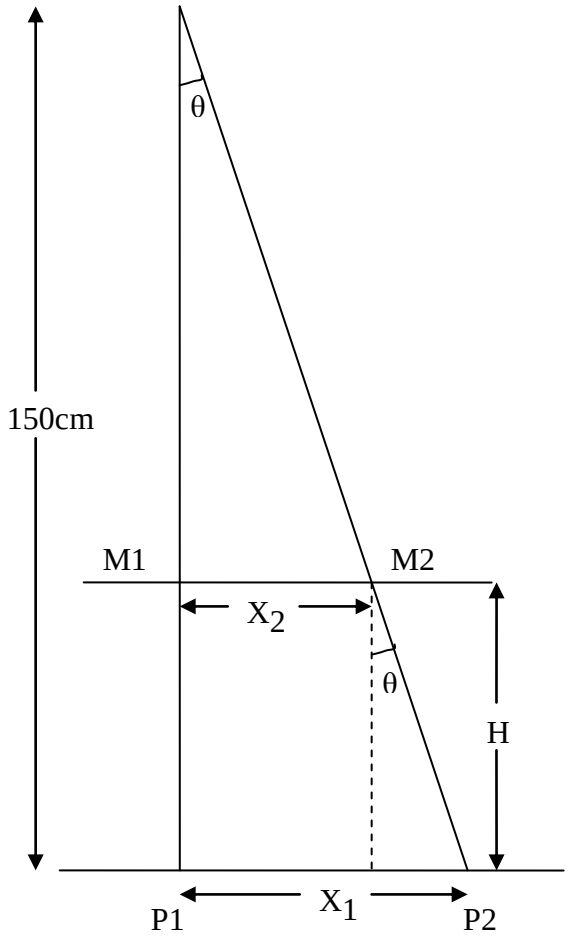

Figure 20: Represents a schematic diagram used to calculate the height

Let's assume M1 is the marker on the axis of the origin and P1 is its projection. M2 represents any other marker along the x-axis or the y-axis with P2 as its projection. The x-ray source is kept at a fixed distance from the detector. This distance can be electronically controlled from the operating console. For the first and second trial this distance was fixed at 150cm and for the third trial it was fixed at 170cm. H represents the height between the markers from the detector plane, X_2 represents the distance between the markers on the marker plane and X_1 represents the distance between the projections of the markers on the detector plane.

When the image is segmented the coordinates of the centroid represent the pixel. This can be converted to centimeters by simply multiplying it with the resolution of the flat panel detector, 0.0388cm. So once the coordinates is converted to centimeters X_1 calculated by subtracting the coordinates of the markers along the x and y axis from the origin. X_2 is physically calculated using a foot ruler.

From the figure Tanθ can be represented by two equations.

$$\text{Tan}\theta = X_2 / (150 - H) \text{ and}$$

$$\text{Tan}\theta = (X_1 - X_2) / H$$

Solving these two equations simultaneously the height of the markers can be calculate using the formula

$$H = 150*(X_1 - X_2)/X_1$$

The above formulae will give the value of H for one marker with respect to the central marker. The same procedure is repeated to calculate the distances between all the

markers and its projections with respect to the selected origin. Using the distance H is calculated for the respective markers and a mean of all the H's is used as the height between the marker plane and the detector plane.

This was the procedure followed for the first and the second trial. For the third trial the x-ray source was placed at a distance of 170cm from the detector. The procedure remains the same for the third trial with the only difference being the change in the formulae for the calculation of H which is $H = 170*(X_1 - X_2)/X_1$

3.3.2 Calculate the Coordinates of the Markers: The same raw image which was used to calculate the height is used to calculate the coordinates of the markers. For all coordinate calculation purposes the center of the detector plane is considered as the origin. For calibration purposes the x-ray source is placed along the z-axis at a height of 150cm. Thus the coordinates of the source is [0, 0, 150]. The height at which the markers are placed represents the z-coordinates of the markers with the x and y coordinates unknown. Thus the coordinates of the markers is [x, y, H]. H is calculated using the formula described earlier. The aim here is to calculate the x and y coordinates of the markers using the coordinates of the projection of the markers on the detector.

Once the image is acquired, it is processed so that it can be segmented and labeled. The centroid for each of the labeled marker is calculated with respect to the origin. The coordinates of the centroid are converter to centimeters using the resolution of the detector. So once the coordinates of the x-ray source, the projection of the markers and the z-coordinate of the markers are known, the 3-D coordinates of the markers can be calculated

using the equation of a line in space. The above process was done using a custom written algorithm implemented using MATLAB and the image processing toolbox.

Figure 21 shows the x-ray source placed at point S [0, 0, 150], two random markers used for calibration C1 and C2 and their projections C3 and C4. From the figure we observe points S, C1 and C3 form a straight line in 3-D.

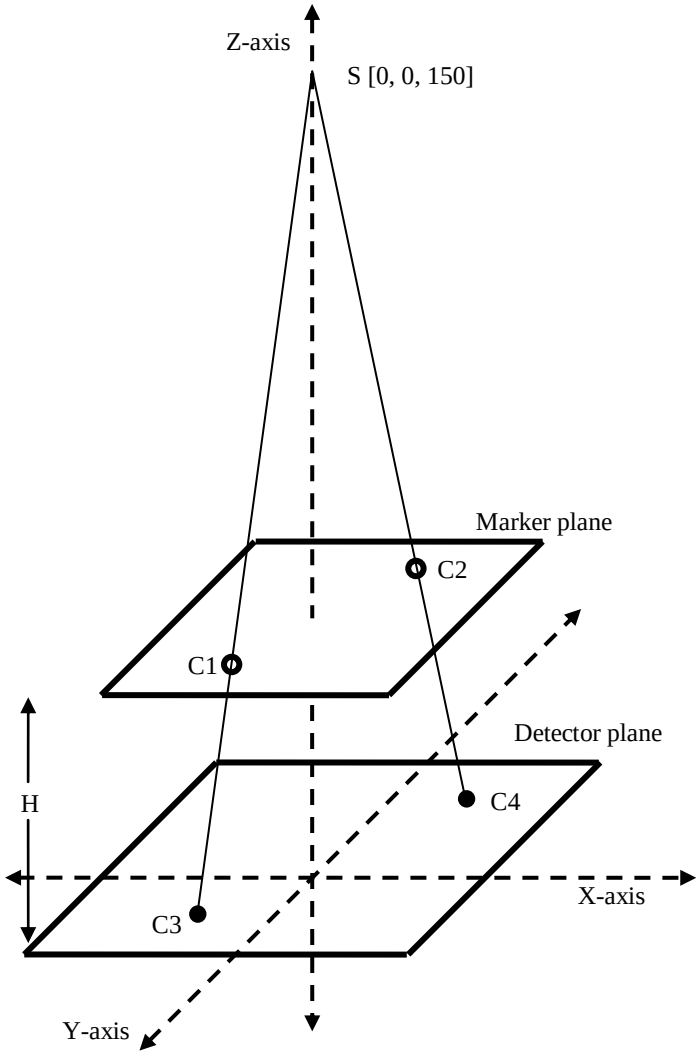

Figure 21: Represents a schematic for the calculating the coordinates of the markers from the calibration image

This line can be represented by the following three parametric equations

$$X = x_1 + t\,(x_2 - x_1)$$
$$Y = y_1 + t\,(y_2 - y_1)$$
$$Z = z_1 + t\,(z_2 - z_1)$$

where t varies from $-\infty$ to ∞

The 3-D coordinates of the source S and the point C3 are known. The z-coordinate for point C1 is also known. Substituting the values of the z-coordinates in the equation for Z we get t = H/150. By substituting the value for t and the values for the x and y coordinate of the source and the projections in the equations of X and Y, the 3-D coordinates of the markers with respect to the origin is calculated.

3.4 Test Plans

Three test plans were created to mimic an actual clinical scenario. The plans were created on the software that controls the afterloader. The idea behind creating a test plan is to know beforehand the exact position of the HDR source and the path it follows. Thus once the exact planned 3-D coordinates of the treatment trials are known, images are acquired using the HDR source and used to reconstruct the source. Thus the accuracy of the system can be checked by comparing the coordinates of the reconstructed source to the coordinates of the planned dwell positions of the treatment plan.

The other aim of the test plans was to test different source – detector distance. We believe 50cm to 70cm is a comfortable distance to place the detector from the patient. From the initial set of images it is observed that good quality images are acquired at these distances. Now what needs to be checked is if the path of the source can be retraced at these distances.

A typical brachytherapy treatment is composed of dwell positions and dwell times. Dwell positions are nothing but distances with respect to a reference point. For all the three plans the tip of the test catheter was consider as the reference point as well as the 1st dwell position.

The afterloader delivers the source from one of its output channels to the test catheter through guided tubes. The test catheter was positioned at the isocenter with the help of laser beams. In radiation physics the isocenter is that point in space through which all the radiation beams intersect and the central beam passes through it. The software of the Acuity machine allows the user to adjust the distance between the isocenter and the detector. This was the reason to place the test catheter at the isocenter. Figure 22 represents the schematic for the test plans.

Following the same system of axes, the tip of the catheter is placed at the isocenter. The system of axes is chosen such that the isocenter falls on the z-axis. So once the catheter is located at the isocenter, the source – detector distance can be adjusted with the help of the simulation software of Acuity. Out of the three test plans the source – detector distance was 50cm for the first and the second plan and 70cm for the third plan.

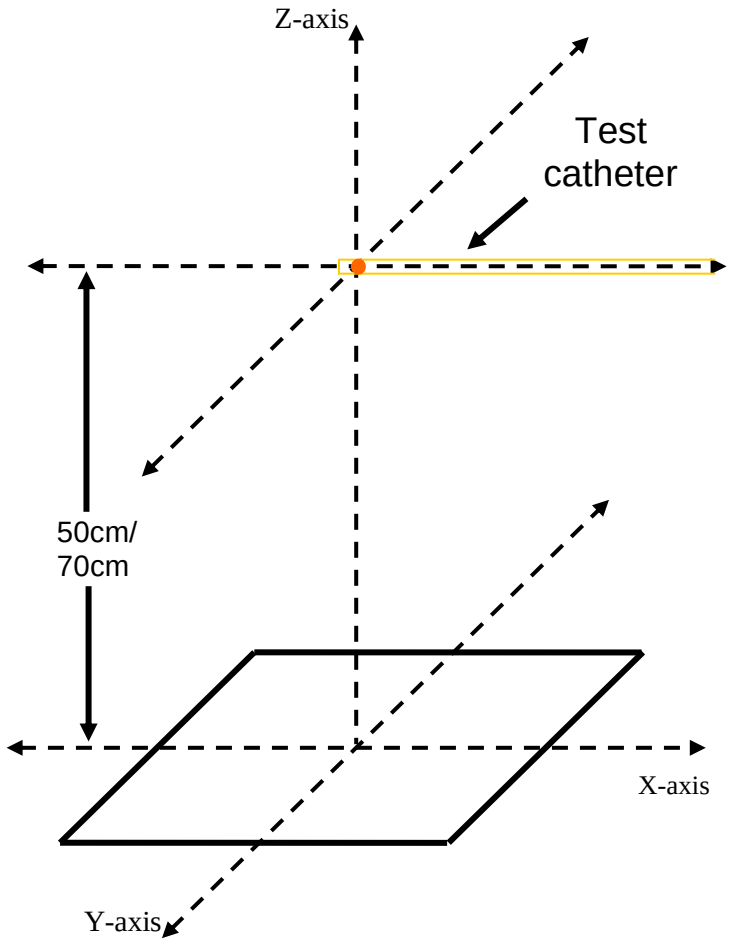

Figure 22: Represents a schematic explaining the positioning of the test catheter and the test plan

The catheter arrangement is placed on the operating couch and the flat panel detector is kept parallel to the couch. The catheter is aligned along the x-axis with its tip on the z-axis at the desired height from the detector. So the source was planned to move only along the x-axis with respect to the tip of the catheter, keeping the y-axis and z-axis constant.

In order to send the HDR source to the 1st planned dwell position by the afterloader, the exact length of the guided tube and the length of the catheter have to be measure. A measuring wire is used to measure the distance the source has to travel from the output channel of the afterloader to the tip of the guide tube. The length of the catheter is added to this distance which gives the start point that the afterloader has to send the HDR source so that it is delivered at the 1st planned position. This is one of the QA procedures and has to be followed before every treatment.

The second component of a typical brachytherapy treatment plan is the dwell time. Dwell time is the amount of time for which the source is said to remain at a given dwell position. The dwell time for all three test plans was set to be sixty seconds for each dwell position. Image acquisition was done manually and it took approximately five seconds to acquire one image. For every dwell position five images were acquired for the first and second trial and six images were acquired for the third trial. Thus the dwell time was chosen to be sixty seconds which gave enough time to manually acquire the images.

3.4.1 First Trial: The plan for the first trial had one applicator with three dwell positions. The dwell time for each position was 60 seconds, with source strength 6.2Ci. The distance between the HDR source and the flat panel detector was 50cm. The plan was simulated such that the afterloader delivers the HDR source to the isocenter for the first dwell position, then 0.5cm away in the x-direction for the second dwell position and lastly 2cm away in the x-direction for the third dwell position. A well defined 9x7 matrix of markers

were used which were spaced 2cm apart from each other. The markers were placed on the plexiglass which was mounted on top of the cover of the detector.

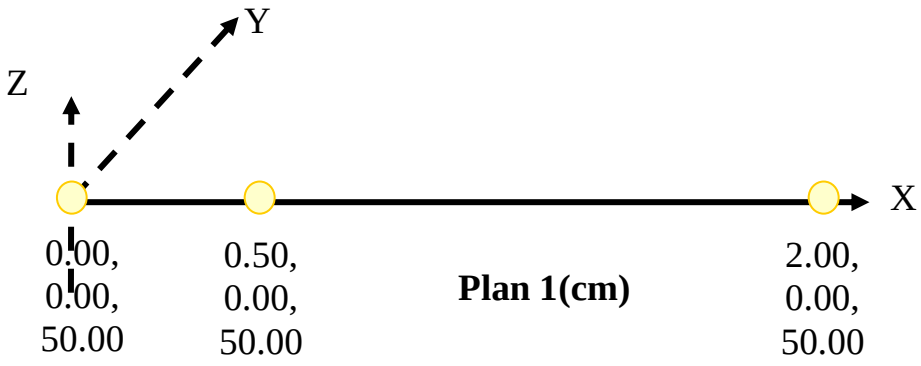

Figure 23: 3D representation of the first test plan

3.4.2 Second and Third Trial: The plan for the second and third trial had one applicator with four dwell positions. The dwell time for each position was 60 seconds, with source strength 6.557Ci. The plan was simulated such that the afterloader delivers the HDR source to the isocenter for the first dwell position, then 0.5cm away in the x-direction for the second dwell position, then 1cm away in the x-direction for the third dwell position and lastly 2cm away in the x-direction for the fourth dwell position. A well defined 8x5 matrix of markers were used which were spaced 2cm apart from each other. The markers were placed on the plexiglass which was mounted on top of the cover of the detector. For the second trial the flat panel detector was placed at a distance of 50cm from the source and for the third trial it was placed at 70cm from the source

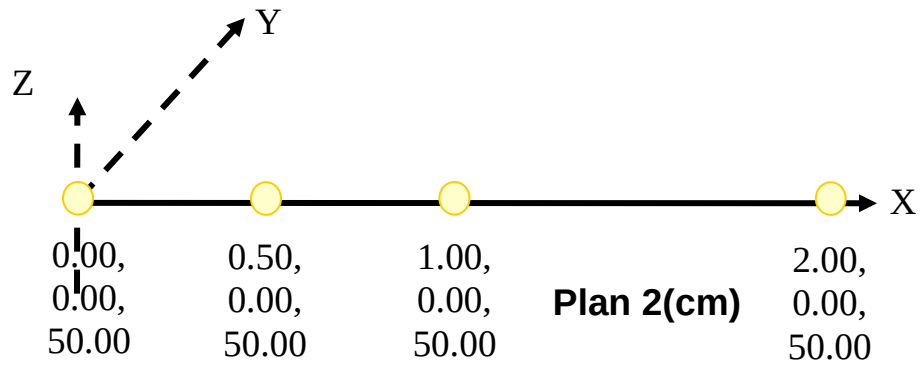

Figure 24: 3D representation of the second test plan

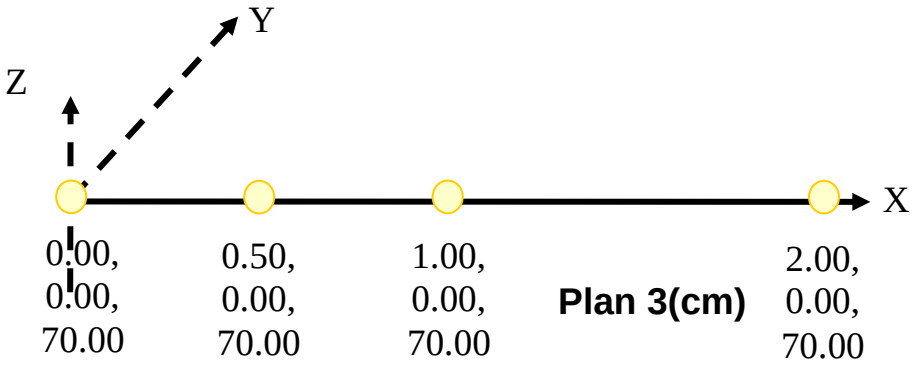

Figure 25: 3D representation of the third test plan

3.5 Image Acquisition

Initially images are acquired using the X-ray source for calibration. After the calibration image is acquired the collimator jaws for the x-ray source are closed shut. In this way during the test trials, even though the x-ray source will be active at the same time,

the only radiation source available for imaging will be the HDR source. Before the test plan is run a blank image is acquired, without the HDR source and with the jaws of the collimator shut. This blank image when subtracted from the image acquired using the HDR source takes into account any kind of exposure and noise produced by leakage x-ray beams.

The next step is to run the test plans and acquire images using the HDR source. Each time the test plans were run, the afterloader will send the HDR source to the planned dwell positions. For each dwell position when the HDR source is active, the exit radiation of the radiation source will produce the projection of the markers on the detector. The dwell time for each dwell position was chosen to be sixty second which gave enough time to manually acquire images (Figure 26).

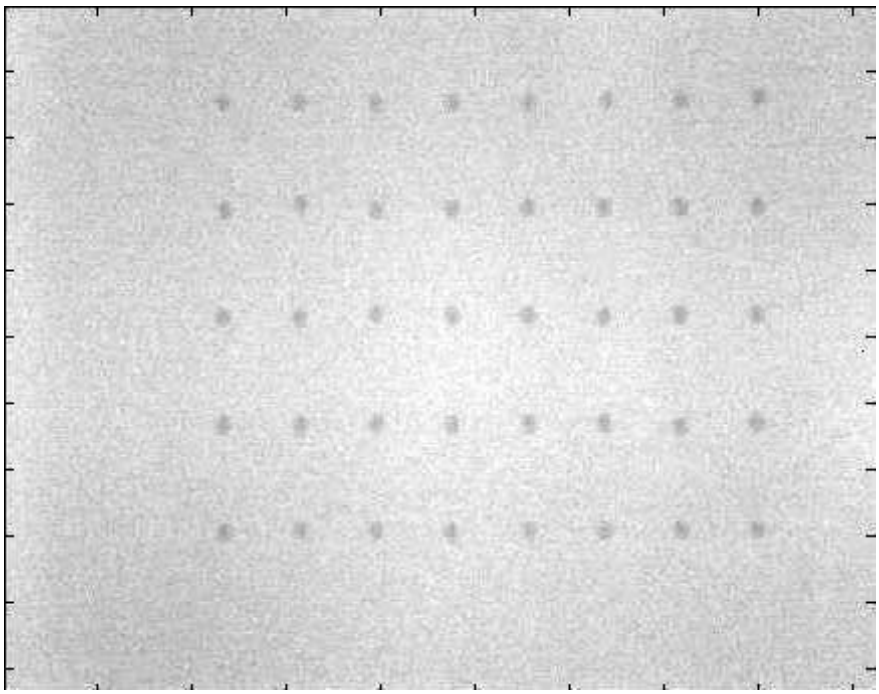

Figure 26: Grey scale image acquired using the HDR source and flat panel detector for the first dwell position of test plan 1

The time required to acquire an image manually is less than ten seconds. Yet the dwell time was chosen to be sixty seconds. The reason behind this lengthy dwell time was to acquire at least five images for every dwell position. The images were acquired and saved using the software for the Acuity machine. From here the images were exported in the DICOM format and read in MATLAB. (code explained earlier in the chapter pg 34)

Averaging over five images helps to reduce the noise in the image. The projection of the markers hold a constant value and noise is assumed to be truly random. The concept of image averaging is that when the five images are added together, the random fluctuations of the noise above and below the projection of the markers will gradually cancel each other out, thus increasing the signal to noise ratio of the image by removing major components of noise.

Even after image averaging unwanted noise was observed along the borders of the image. This noise was consistent for all the images and was removed by simply cropping twenty five pixels off each border of the image. Figure 26 depicts a grey scale image after being averaged and cropped, of the image acquired for the first dwell position of the second test plan.

```
I=X(26:743,26:999);
```

where X is the original images after image averaging and the cropped image is stored in I.

3.6 Morphological Image Processing

Once the images are acquired, they are exported in the DICOM format so that these images can be processed in MATLAB. The images are read in MATLAB, then averaged, subtracted and cropped (figure 26). This image is then processed in order to acquire the 3-D coordinates of the projection of the markers. The centroids of the projection of the marker on the acquired images are used as surrogates for the 3-D coordinates. Even after image averaging and cropping of the image noise still exists in the grey scale image which needs to be eliminated inorder to isolate the markers in the image.

The shape and size of the markers that have to be isolated from the image are known before hand. For this reason morphological image processing is performed to isolate the projection of the markers and obtain the coordinates of the centroid. The '*imbothat*' command from the MATLAB image processing toolbox was used to perform morphological bottom-hat filtering on the grayscale image. The bottom-hat filter requires a structuring element which would define the shape of the markers. The markers are circular structures, so the first step is to define a structuring element of the type 'disk'. This is done by using the '*strel*' function. The filtered image is then stored in a variable. An example of the *imbothat* and *strel* function is explained below,

```
se = strel('disk',25);
I1 = imbothat(I,se);
```

The above code creates a flat, disk-shaped structuring element ‘se’ with a radius of 25 pixels. The bottom-hat function is performed on the cropped image I using ‘se’ and stores it in I1.

Other than the bottom-hat filter two more filters were used in order to reduce noise. First a wiener2 filter was used. Wiener2 is a 2-D pixelwise adaptive Wiener filtering method which acts as a lowpass filter to improve a degraded grayscale image by removing the noise. It is based on statistics estimated from a local neighborhood of each pixel. Next a medfilt2 filter was used. Medfilt2 is a 2-D nonlinear median filtering method which is used to reduce the ‘salt and pepper’ noise. The code for the two filters is explained below,

```
[I2,noise] = wiener2(I1,[15 15]);
I3 = medfilt2(I2,[8 8]);
```

A 15x15 pixel size neighborhood was used to estimate the local image mean and standard deviation to perform the wiener2 filtration method on the image I1 and the filtered image was stored in I2. A 8x8 pixel size neighborhood was used around each pixel in I2 to perform the median filtration method and the filtered images was stored in I3.

The next step is to isolate the markers. The grayscale image is converted into a binary image such that only the markers take the value 1 while the rest of the image is 0. This is done by applying a threshold to the image.

```
I4 = I3>mean2(I3) + 2.5*std2(I3);
```

The mean value plus 2.5 times the standard deviation value was used as the threshold applied to image I3 and the binary image was stored in I4. From the binary image I4 the

markers can be isolated, labeled and the centroids for each marker can be calculated using the code as described below,

```
[I5,NUM] = bwlabeln(I4);
STATS = regionprops(I5,'Centroid','Area');
```

The '*bwlabeln'* function labels the markers in image I4 and saves it in I5. The 'regionprops' function measures the centroid and area of the labeled markers in image I5 and stores it in the array STATS. The x-y pixel coordinates of the centroids can be accessed using the Comma-Separated List Syntax as explained below,

STATS.Centroid

The centroid acts as a substitute for the coordinates of the markers and is represented by the pixel number. In order to obtain the coordinates with respect to the system of axis chosen by us, the x and y coordinates of the pixel number of the centroid have to be subtracted by the center of the detector. The coordinates are converted into centimeters by multiplying the pixel number with the pixel size or the resolution of the flat panel detector. For all the experiments the detector was set at half resolution with a pixel size of 0.0388cm. Converting pixel numbers to centimeters simplified calculations for the reconstruction of the source. The same procedure was carried out for the calibration image and the 3-D coordinates of the markers were also converted into centimeters. Figure 27 depicts a segmented and labeled image which was acquired for the first dwell position of the second test plan.

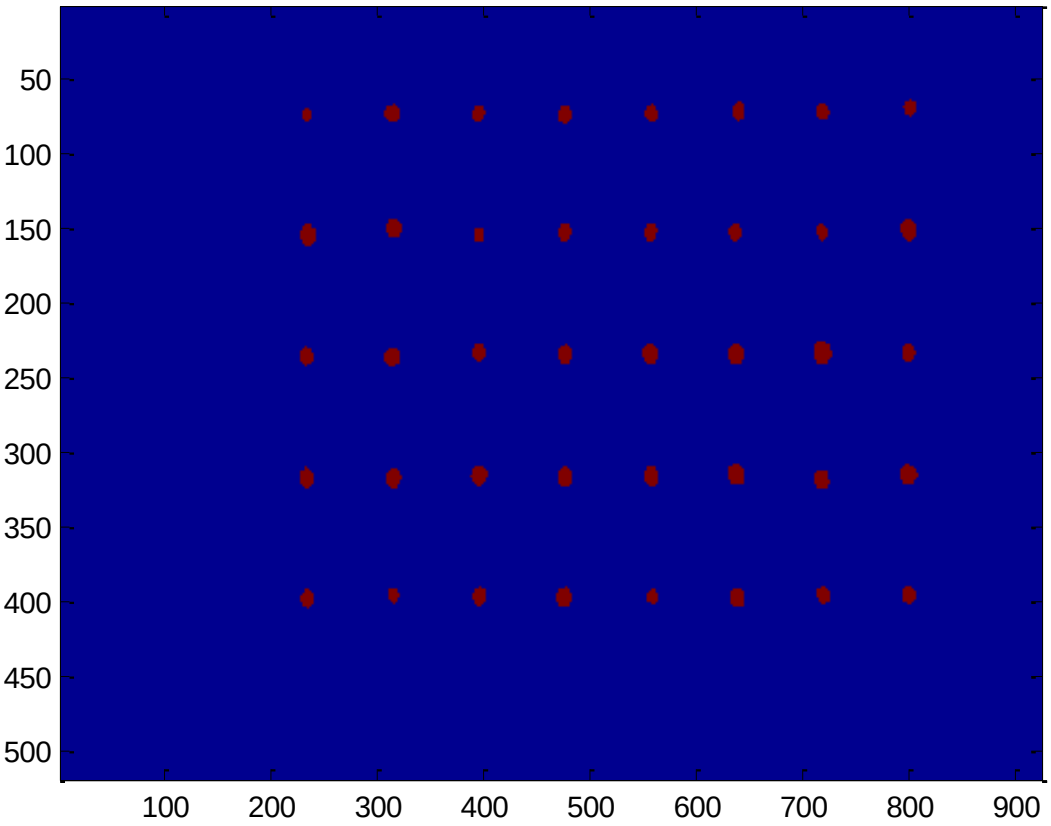

Figure 27: Binary image obtained after morphologically processing and segmenting the grey scale image

3.7 Reconstruction of the Source

On investigating the images for all the dwell positions for all the test plans it was observed that the coordinates of the projections of the markers is unique for each dwell position. This demonstrates that the coordinates of the projection of the markers are correlated to the position of the source. The calibration method gives the exact 3-D coordinates of the markers. The exact 3-D coordinates of the projection of the markers are

obtained by processing the images acquired using the HDR source. Using these 3-D coordinates of the markers and the projection, the position of the source is formed by pairing each marker with its projection and calculating the shortest distance. This is done by providing a label to each blob on the marker image and the projection image and with the help of the label number the marker is paired with its respective projection.

When the labeling of the segmented image is performed, the markers get labeled in any random order. Thus the labeled markers needs to be rearrange such that we have the same order for the markers on the calibration image and the projection of the markers on the image acquired by the HDR source. This makes the pairing of the markers with its respective much easier. This is done by using the 'sort' command in MATLAB. The sorted coordinates of the projections are stored in a variable called 'img' while the sorted coordinates of the markers are stored in a variable called 'cal'.

Lines in 3-D are defined with the help of the 3-D coordinates of the markers and its respective projections. Two lines defined by two marker – projection pair is used at one time. The intersection of the two lines gives us the position of the source. The intersection of two lines in 3-D is very unlikely. Instead the shortest line segment which connects the two lines in 3-D was compute. This line segment is unique and is considered to be the intersection of the two lines.

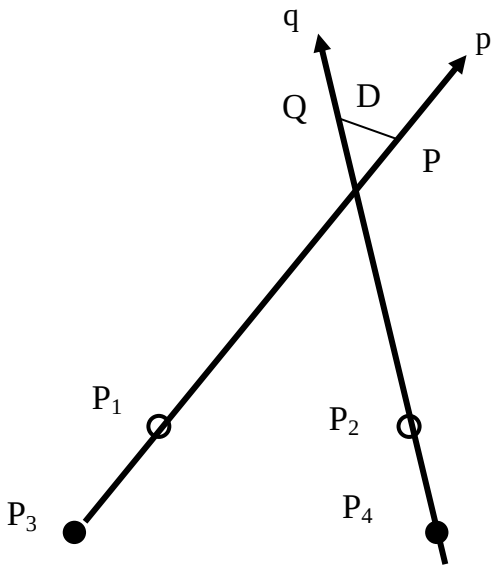

Figure 28: Schematic explaining intersection of two lines in 3D

From the figure 28, line p is defined by the marker P_1 and its projection P_3 and represented by equation 1; line q is defined by the marker P_2 and its projection P_4 and is represented by equation 2

$$P = P_1 + mu_p * (P_3 - P_1) \text{ …….. (1)}$$
$$Q = P_2 + mu_q * (P_4 - P_2) \text{…….. (2)}$$

P and Q represent the points on the lines p and q which give the shortest distance between the two lines. The values of mu_p and mu_q range from negative infinity to positive infinity.

The shortest line segment between the two lines should be perpendicular to the two lines. Thus two equations for the dot product are represented as

$$(P - Q) \text{ dot } (P_3 - P_1) = 0$$
$$(P - Q) \text{ dot } (P_4 - P_2) = 0$$

Expanding the above equations using 1 and 2 we get,

$$(P_1 - P_2 + mu_p*(P_3 - P_1) - mu_q*(P_4 - P_2)) \text{ dot } (P_3 - P_1) = 0$$
$$(P_1 - P_2 + mu_p*(P_3 - P_1) - mu_q*(P_4 - P_2)) \text{ dot } (P_4 - P_2) = 0$$

The two equations above represents two equations with two unknowns mu_p and mu_q, thus solving the above two equations simultaneously gives the values of mu_p and mu_q. The coordinates of P and Q is derived by substituting these values in equations 1 and 2. The mean of P and Q is used as the position of the source.

Thus the above procedure is repeated for all possible combination of marker – projection pairs. Thus N markers would produce N * (N-1) / 2 combinations of marker – projection pairs, each pair giving a shortest distance D and a P and a Q, and a mean over all the P's and Q's will give the most accurate position of the source.

All of the above was implemented using MATLAB. Right from reading the five dicom images, the calibration image and the blank image, to image averaging and subtraction for noise cancelation, to calibrating the system, to segmenting and labeling the HDR image, calculating the coordinates for the calibration and HDR images, sorting out the labeled images, pairing the markers with its respective projection and finally calculating the shortest distance and the coordinates for the points of intersection, to ultimately give the 3-D coordinates of the position of the source for each dwell position was implemented in one automated code in MATLAB.

Chapter 4 Results

The three test plans are run and images for each dwell position are acquired for all the three test plans. The data analysis is carried out as explained above using MATLAB. The same procedure is carried out for each dwell position of every test plan. The acquired images act as input data for the MATLAB code and the output of the program gives three results; shortest distance D : the mean of N * (N-1) / 2 (where N is the number of markers used for the experiment) values of the shortest distance and its standard deviation, variable P : mean of N * (N-1) / 2 values of one of the end points making up the shortest distance and its standard deviation, variable Q : mean of N * (N-1) / 2 values of the other end point making up the shortest distance and its standard deviation.

Once images are acquired the height (H) between the markers and the detector needs to be calculated. This is achieved using the formulae

$$H = D*(X_1 - X_2)/X_1$$

Where D is the distance between the x-ray source and the detector. The method is explained in chapter 3. Table 1 gives the calculated distance of H for the three test plans.

Using the calculated height between the markers and the detector, the 3D coordinates of the markers is calculated from the images acquired for each dwell position and the calibration image using the MATLAB code and each marker properly paired with

Distance between HDR source and detector	Distance between marker and detector
50cm	25.49cm
70cm	25.57cm

Table 1: Height between marker and detector

its projection. Method is explained in chapter 3. Figure 29 represents the 3D pot of the marker-projection pairs for the first dwell position of the second plan.

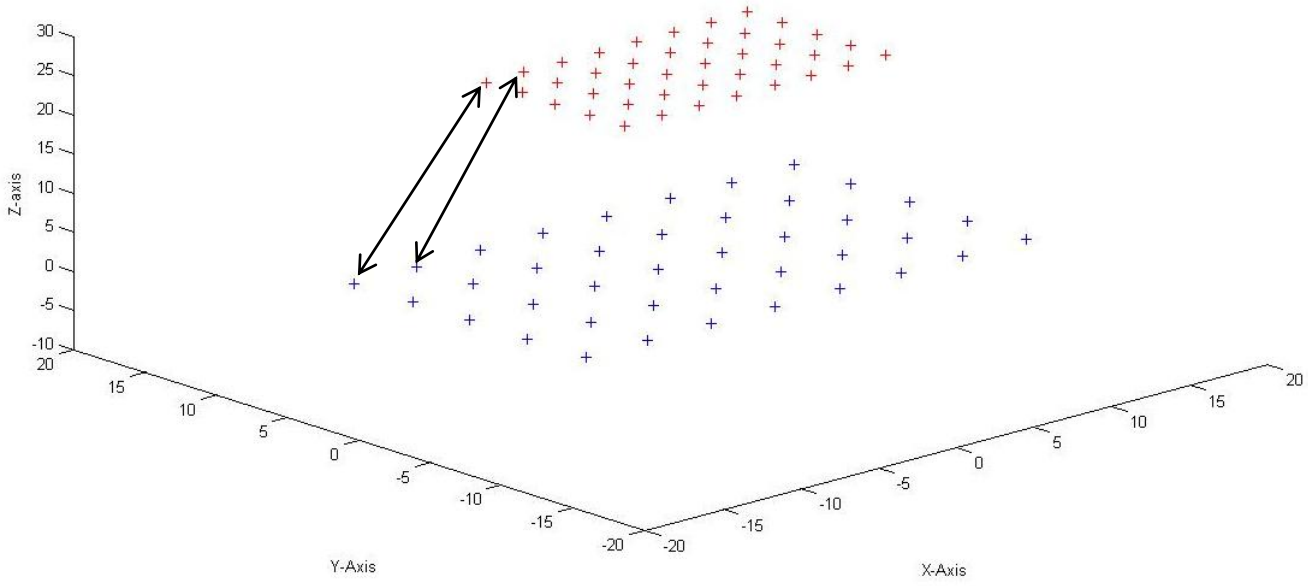

Figure 29: 3D plot of the markers and its projection for the first dwell position of the second test plan

The 3D coordinates of each marker along with its projection defines a line in space. Combinations of two lines are chosen and the intersection of these two lines will produce the planned dwell position of the HDR source, that is, a P and a Q. For example the

intersection of lines produced by markers 1 and 2 will give P with coordinates [0.3654 -0.2324 50.6766] and Q with coordinates [0.3654 -0.2331 50.6764]. 40 markers along with its projections will define 40 lines which will produce 720 such combinations, resulting in 720 P's and 720 Q's. Similarly P's and Q's are calculated for every dwell position in all the three plans.

Figure 30 represents a scatter plot of all the P's and Q's for test plan 2. The blue dots represent the P's and pink dots represent the Q's. The black dot represents the mean of P and Q. From the figure it can be observed that the uncertainties along the Z-axis are considerably higher as compared to the X and Y axis.

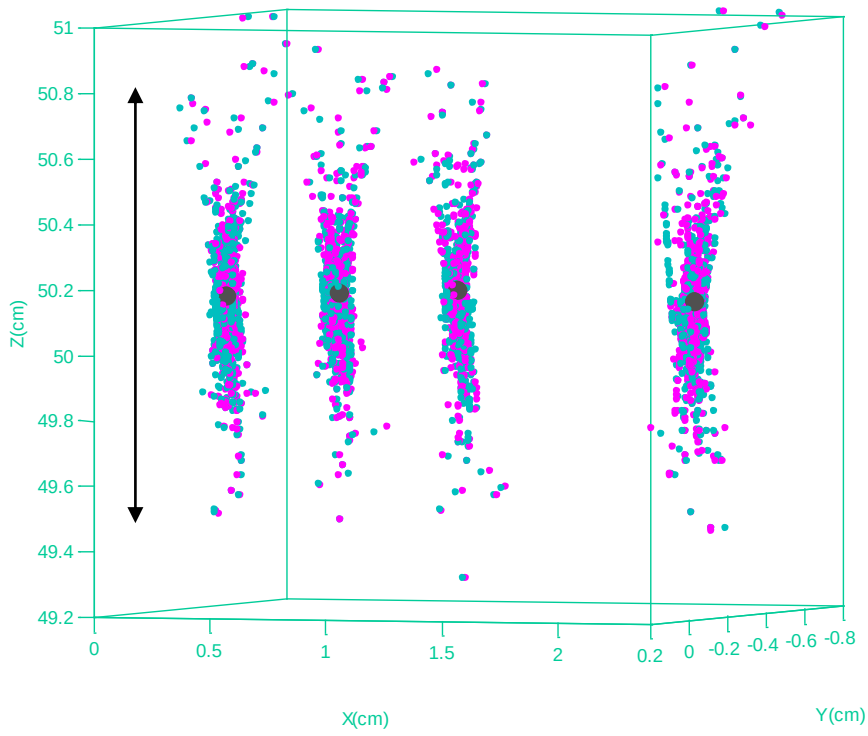

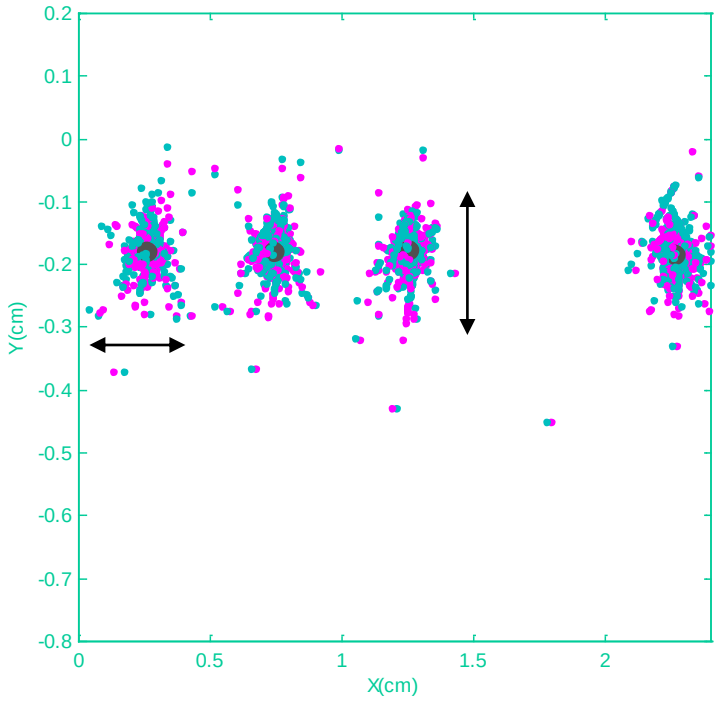

Figure 30: Scatter plot of P's and Q's for Test Plan 2

Table 2,3,4 represents the mean and standard deviation values of the D's, P's and Q's for all the three test plans for each dwell position. P and Q represent the x-coordinate, y-coordinate and z-coordinate in the form [X Y Z]. The values of D, P and Q have the unit's centimeters.

		D(cm)	P(cm)	Q(cm)
1st Position	**Mean**	**0.0261**	**[0.3262 -0.2646 50.1297]**	**[0.3251 -0.2699 50.1304]**
	Std Div	0.0170	[0.0306 0.0231 0.1386]	[0.0342 0.0219 0.1386]
2nd Position	**Mean**	**0.0272**	**[0.8230 -0.2733 50.1062]**	**[0.8229 -0.2767 50.1066]**
	Std Div	0.0177	[0.0245 0.0189 0.1160]	[0.0263 0.0212 0.1161]
3rd Position	**Mean**	**0.0216**	**[2.3125 -0.2680 50.0535]**	**[2.3071 -0.2763 50.0539]**
	Std Div	0.0153	[0.0236 0.0152 0.0912]	[0.0242 0.0187 0.0907]

Table 2: Mean and standard deviation of the shortest distance D and the x, y and z coordinates of points P and Q for Test Plan 1 for each dwell position

		D(cm)	P(cm)	Q(cm)
1st Position	**Mean**	**0.0239**	**[0.2598 -0.1781 50.1625]**	**[0.2606 -0.1827 50.1621]**
	Std Div	0.0184	[0.0342 0.0275 0.1795]	[0.0316 0.0237 0.1799]
2nd Position	**Mean**	**0.0251**	**[0.7417 -0.1775 50.1780]**	**[0.7392 -0.1804 50.1756]**
	Std Div	0.0206	[0.0339 0.0282 0.1748]	[0.0347 0.0265 0.1746]
3rd Position	**Mean**	**0.0243**	**[1. 2642 -0.1764 50.1901]**	**[1. 2645 -0.1799 50.1921]**
	Std Div	0.0194	[0.0303 0.0270 0.1821]	[0.0317 0.0277 0.1815]
4th Position	**Mean**	**0.0285**	**[2.2677 -0.1830 50.1611]**	**[2. 2637 -0.1849 50.1307]**
	Std Div	0.0227	[0.0430 0.0317 0.2058]	[0.0416 0.0291 0.2060]

Table 3: Mean and standard deviation of the shortest distance D and the x, y and z coordinates of points P and Q for Test Plan 2 for each dwell position

		D(cm)	P(cm)	Q(cm)
1st Position	**Mean**	**0.0261**	**[0.2400 -0.1375 70.1254]**	**[0.2431 -0.1349 70.1254]**
	Std Div	0.0198	[0.0319 0.0257 0.3197]	[0.0344 0.0264 0.3194]
2nd Position	**Mean**	**0.0238**	**[0.7352 -0.1385 70.1774]**	**[0.7352 -0.1378 70.1772]**
	Std Div	0.0185	[0.0344 0.0263 0.3469]	[0.0335 0.0270 0.3468]
3rd Position	**Mean**	**0.0338**	**[1. 2437 -0.1374 70.1827]**	**[1. 2400 -0.1382 70.1823]**
	Std Div	0.0264	[0.0404 0.0364 0.4320]	[0.0409 0.0326 0.4320]
4th Position	**Mean**	**0.0276**	**[2.2239 -0.1403 70.1833]**	**[2. 2223 -0.1385 70.1830]**
	Std Div	0.0222	[0.0394 0.0266 0.3838]	[0.0419 0.0274 0.3837]

Table 4: Mean and standard deviation of the shortest distance D and the x, y and z coordinates of points P and Q for Test Plan 3 for each dwell position

The mean values of P and Q is used to estimate the 3D coordinates of the position of the source. Thus for every dwell position of each test plan the average of the 3D coordinates of P and Q is considered as the reconstructed 3D coordinates of the HDR source. Using the above three tables the HDR source can be reconstructed in 3D. First the mean values of P and Q are narrowed down to two decimal places for each dwell position and then averaged in order to acquire the reconstructed coordinates of the HDR source. Figure 31 represents the 3D coordinates of the reconstructed dwell position of the HDR source.

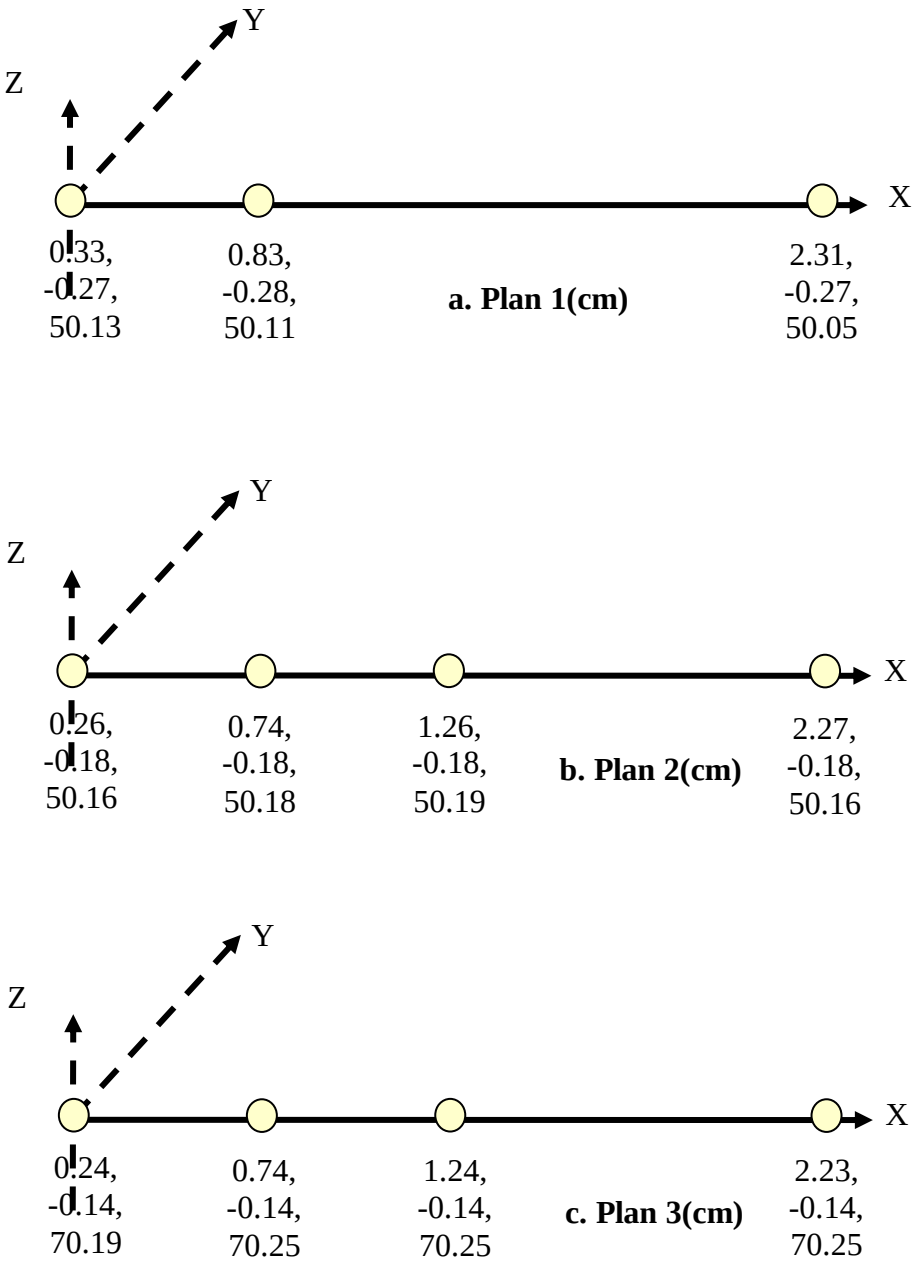

Figure 31: Representation of the reconstructed 3D coordinates of the dwell position for (a) Test Plan 1, (b) Test Plan 2 and (c) Test Plan 3

On comparison of the reconstructed 3D coordinates to the planned dwell positions, it is observed that there exists an off set for the first dwell position. This can occur as the initial position of the source was manually placed along the x and y axis with the help of lasers. Uncertainties along the z-axis are explained later. From the figure 30 it is observed that the value for the y-coordinates for all the three plans is consistent for each plan. This confirms that an offset exists and the source was not exactly placed at [0 0 Z].

It is know from the test plans that the source was moved only along the x-axis by a known amount, keeping the y-axis at zero and the z-axis at a constant height either 50cm or 70cm. A dwell position in the treatment plan is defined as a distance measured from the tip of the wire holding the radiation source. Thus in order to make the results comparable to the test plans, the 3D coordinates of the reconstructed plan need to be converted into distances with respect to the tip of the wire which in this case is the origin. This is done by calculating the distances for every dwell position with respect to the origin. For our calculations for the first plan, the dwell position with the coordinates [0.33 -0.27 50.13] is considered as the origin and all other distances are calculated with respect to this point. Similar calculations are carried out for the second with initial point as [0.26 -0.18 50.16] and for the third plan with initial point as [0.24 -0.14 70.19]. Distances are calculated using the Euclidean distance equation for points in 3D which is

$$\text{Distance} = \text{sq root } \{(x_1 - x_0)^2 + (y_1 - y_0)^2 + (z_1 - z_2)^2\}$$

Where (x_0, y_0, z_0) represent the initial point and

(x_1, y_1, z_1) represents the point till where the distance has to be calculated

The planned dwell positions can now be compared to the reconstructed dwell positions as shown below.

	Planned dwell position (cm)	Reconstructed dwell position (cm)	Error (cm)
Plan 1	0.00	0.00	
	0.50	0.50	0.00
	2.00	1.99	0.01
Plan 2	0.00	0.00	
	0.50	0.48	0.02
	1.00	1.00	0.00
	2.00	2.01	0.01
Plan 3	0.00	0.00	
	0.50	0.50	0.00
	1.00	1.00	0.00
	2.00	1.99	0.01

Table 5: Comparison of planned dwell position against reconstructed dwell position

From table 5 defines the reconstructed dwell positions in centimeters with respect to the initial position. The test plans were defined such that radiation source 0.5cm, 1cm or 2cm from the initial point. From table 6 one can easily compare the planned dwell position against the reconstructed dwell position and it is observed that the reconstructed dwell position was within ±0.02cm of the planned dwell position.

For the above comparison to be made it is very important to have a gold standard measuring method to check the accuracy of the planned dwell positions against which the reconstructed dwell position is being compared. The brachytherapy imaging suite is equipped with a high zoom camera. The test catheter used was transparent, thus the movement of the wire within the catheter can be seen with the help of the camera. The accuracy of the planned dwell position was visually checked by placing a ruler along the catheter (with 1mm as the smallest dimension on the ruler) and verifying the placement of the source by watching the movement of the catheter on the display monitor of the camera.

CHAPTER 5 Discussion

In this study the HDR Ir-192 source was used as an imaging source to acquire images of a well defined matrix of markers. These images were processed using a software code written in MATLAB to locate the 3D position of the HDR source. The results from this study have demonstrated that the HDR source can be tracked with a sensitivity of ± 0.02cm using the images acquired of the projections of the markers mounted on top of the cover of the flat panel detector.

This method is easy to accommodate in the current method of treatment as it only requires the addition of a plexiglass mount with a matrix of markers embedded in it that is added to the cover of the flat panel detector. One important characteristic of the study is the placement of the flat panel detector and the matrix of markers such that the arrangement does not interfere with the treatment delivery process and the comfort of the patient. For this reason the set-up was tested for various distances the detector can be placed from the source which in the actual clinical trial would be present inside the patient. The results proved that this method can be used for a source detector distance ranging from 50cm to 70cm, which would provide enough room for the treatment to be carried out smoothly.

This method utilizes the exit radiation of the HDR source alone for tracking the radiation source without the requirement of another radiation source. The X-ray source is

only required during calibration procedures. This is another important characteristic of this study because the patient will not be exposed to any additional radiation does.

For this study the Acuity machine was employed in the clinical mode, which means the flat panel detector would be active only when the X-ray source is in the ON mode. The Acuity machine has the option of blocking the X-rays by closing the collimator jaws of the X-ray source. By doing so the flat panel detector will not be exposed to the X-rays, leaving the HDR source as the sole radiation source for imaging.

The Nuclear Regulatory Commission (NRC) regulation prohibits the use of two radiation source at the same time for a radiation therapy treatment. In order for this method to abide by the NRC regulations images have to be acquired by the flat panel detector using the Acuity machine in the non-clinical mode. This means the X-ray source cannot be active during the radiation therapy treatment. Under the test conditions created in this study the dwell time was programmed to 60 seconds so that images can be acquired manually. A typical brachytherapy treatment contains dwell times ranging from milliseconds to 100's of seconds. Thus in order to track the source for dwell positions with small dwell times a faster and automated method for acquiring the images is required. The two problems discussed above can be solved by using the IAS Monitor software for the Acuity machine. By doing so, images can be acquired directly from the flat panel detector without exciting the X-ray source at rates as fast as thirty frames per second.

In the final results table (Table 6), the gold standard used to verify the accuracy of the planned dwell position was a visual test, where in a high zoom camera was focused on the transparent catheter and a ruler with 1mm accuracy was placed beside the catheter.

This cannot be followed during actual treatment delivery as the source is present inside the body of the patient. In that case a new gold standard is required against which the reconstructed dwell position can be compared.

Every treatment plan that is created using the BrachyVision software contains a file for the plan in the DICOM format. This file contains the list of applicators and the 3D coordinates for each dwell position of all the applicators that are sent to the afterloader. This file for the plan can be easily exported using the treatment planning system and processed in MATLAB. These 3D coordinates acquired from the treatment planning system will act as the new gold standard against which the reconstructed dwell positions will be compared. In order for this comparison to be made, both the 3D coordinates need to be represented in the same system of axes. For this reason a translation and rotation factor will have to be added to the reconstructed dwell position.

The most important function of the calibration procedure (explained in Chapter 3 pg 40) is calculating the height (H) between the markers and the detectors and this acts as the z-coordinate for the marker position. Any error in this calculation will lead to errors propagating through the entire model for the reconstruction of the source. The formula for calculating the height is $H = D*(X_1 - X_2)/X_1$. Calculation of H requires the central marker (figure 19 pg 41) to coincide with the center of the detector. If this is not true the formula used to calculate the height will have to compensate for angular errors. X_2 is the distance between the markers on the mount. The mount used for the study was not precision built which meant the distance between the markers was not exactly 2cm and could lead to an error in calculating $(X_1 - X_2)$. D (150cm – 170cm) is very large as compared to $(X_1-X_2)/X_1$

(≈0.125cm). Thus a small error in $(X_1-X_2)/X_1$ will lead to a significant error in the calculation of H. In order to minimize this error, the mean value over all the calculated heights is applied. This is reflected in table 1 (pg 62) where the calculated height for 50cm and 70cm differs by 0.1cm.

The scatter plot for the reconstructed P and Q coordinates (Figure 30 pg 64) and result table 4 show the standard deviation along the z-axis is almost ten times greater than the deviation along the x and y axis. The two reasons that can explain the above behavior is an error in calculating H and the current design of the mount. The design of the mount is not sturdy enough to maintain the surface of the mount holding the markers perfectly parallel to the surface of the detector. This implies the z-coordinate for the markers would be different for each marker. The software assumes the surface of the marker plane to be perfectly parallel to the surface of the detector and assigns the calculated height H as the z-coordinate for all the markers in the marker-projection pair (Table 2 pg 66). Calculations for the reconstruction of the HDR source are performed based on these values.

In order to minimize the uncertainties along the z-axis for the reconstructed dwell position improvements in the design for the mount is required with the aim to maintain the marker plane parallel to the detector plane along with better calibration procedures for the calculation of height H. As discussed above errors in calibration occur due to errors in calculating the distances between the markers and the central markers not coinciding with the center of the detector. The first error can be minimized by introducing precision markings for the markers in the new design for the mount. Images can be acquired using x-ray by placing the mount on the surface of detector and the distances between the markers

can be calculated using the segmentation software. The distances between the markers can be manually measured with high accuracy using a precision measuring instrument such as a digital caliper. Comparing these two measurements will give a multiplying factor based on which an accurate measurement of the distances can be achieved. Introduction of a second plane with a single marker in the form of a cross or a hollow disc right above the central marker can help in aligning the x-ray source, the central marker and the center of the system of axis.

The improved design should utilize a stronger and thicker material for the manufacturing of the mount and built to the exact dimensions of the cover of the detector. The design should also include precision markings for the BB's along with provisions for an additional surface with the desired marker for calibration purposes. The new design will help to minimize the errors discussed above.

This study has proved that the source can be tracked using the radiation of the HDR source for imaging a matrix of markers with a sensitivity of ±0.02cm. With the above improvements in place this method can be utilized to track the HDR source in real time, compare it with the dwell position of the treatment plan and if required make the necessary chances, thus making this method an ultimate Quality Assurance procedure for brachytherapy treatments.

Literature Cited

Reference List

(1) Jean-Jacques Mazeron, Alain Gerbaulet. The centenary of discovery of radium. *Radiotherapy and Oncology.* 1998;49:205-216.

(2) Cooper MR. Mastectomy from the perspective of a medical oncologist. *Cancer.* 1994;74:362-365.

(3) Garfinkel L, Boring CC, Heath CW, Jr. Changing trends. An overview of breast cancer incidence and mortality. *Cancer.* 1994;74:222-227.

(4) Austoker J. Screening and self examination for breast cancer. *BMJ.* 1994;309:168-174.

(5) Subir Nag, MD. A Brief History of Brachytherapy. *American Brachytherapy Society, Online Article* 2010.

(6) Kuerer HM, Julian TB, Strom EA et al. Accelerated partial breast irradiation after conservative surgery for breast cancer. *Ann Surg.* 2004;239:338-351.

(7) Ely S, Vioral AN. Breast cancer overview. *Plast Surg Nurs.* 2007;27:128-133.

(8) Schmidt-Ullrich PN, Todor DA, Cuttino LW, Arthur DW. Virtual planning of multicatheter brachytherapy implants for accelerated partial breast irradiation. *Conf Proc IEEE Eng Med Biol Soc.* 2004;5:3124-3127.

(9) Nath R, Anderson LL, Meli JA, Olch AJ, Stitt JA, Williamson JF. Code of practice for brachytherapy physics: report of the AAPM Radiation Therapy Committee Task Group No. 56. American Association of Physicists in Medicine. *Med Phys.* 1997;24:1557-1598.

(10) Kubo HD, Glasgow GP, Pethel TD, Thomadsen BR, Williamson JF. High dose-rate brachytherapy treatment delivery: report of the AAPM Radiation Therapy Committee Task Group No. 59. *Med Phys.* 1998;25:375-403.

(11) Das RK, Bradley KA, Nelson IA, Patel R, Thomadsen BR. Quality assurance of treatment plans for interstitial and intracavitary high-dose-rate brachytherapy. *Brachytherapy.* 2006;5:56-60.

(12) TARA PARKER-POPE. When Radiation Treatment Turns Deadly. *New York Times Article*. 2010

(13) WALT BOGDANICH. Radiation Offers New Cures, and Ways to Do Harm. *New York Times Article.* 2010.

(14) Hart IR, Fidler IJ. Cancer invasion and metastasis. *Q Rev Biol.* 1980;55:121-142.

(15) Draper L. Breast cancer: trends, risks, treatments, and effects. *AAOHN J.* 2006;54:445-451.

(16) American Cancer Society. What is Breast Cancer. *Online Article.* 2010.

(17) Bishop DT. BRCA1 and BRCA2 and breast cancer incidence: a review. *Ann Oncol.* 1999;10 Suppl 6:113-119.

(18) Cotlar AM, DuBose JJ, Rose DM. History of surgery for breast cancer: radical to the sublime. *Curr Surg.* 2003;60:329-337.

(19) Winchester DP, Trabanino L, Lopez MJ. The evolution of surgery for breast cancer. *Surg Oncol Clin N Am.* 2005;14:479-98, vi.

(20) Sakorafas GH, Safioleas M. Breast cancer surgery: an historical narrative. Part I. From prehistoric times to Renaissance. *Eur J Cancer Care (Engl).* 2009;18:530-544.

(21) Madden JL, Kandalaft S, Bourque RA. Modified radical mastectomy. *Ann Surg.* 1972;175:624-634.

(22) Sakorafas GH, Safioleas M. Breast cancer surgery: an historical narrative. Part III. From the sunset of the 19th to the dawn of the 21st century. *Eur J Cancer Care (Engl).* 2010;19:145-166.

(23) Richard M.Levy. Medical Uses of Liner Accelerators. 2010.

(24) Veronesi U, Cascinelli N, Mariani L et al. Twenty-year follow-up of a randomized study comparing breast-conserving surgery with radical mastectomy for early breast cancer. *N Engl J Med.* 2002;347:1227-1232.

(25) Fisher B, Jeong JH, Anderson S, Bryant J, Fisher ER, Wolmark N. Twenty-five-year follow-up of a randomized trial comparing radical mastectomy, total mastectomy, and total mastectomy followed by irradiation. *N Engl J Med.* 2002;347:567-575.

(26) Willers H, Held KD. Introduction to clinical radiation biology. *Hematol Oncol Clin North Am.* 2006;20:1-24.

(27) Kuske RR, Jr. Breast brachytherapy. *Hematol Oncol Clin North Am.* 1999;13:543-vii.

(28) Keynes G. Conservative Treatment Of Cancer Of The Breast. 2, 643-647. 10-2-1937. *Br Med J.*

(29) Dirbas FM, Jeffrey SS, Goffinet DR. The evolution of accelerated, partial breast irradiation as a potential treatment option for women with newly diagnosed breast cancer considering breast conservation. *Cancer Biother Radiopharm.* 2004;19:673-705.

(30) White JR, Wilson JF. Brachytherapy and breast cancer. *Semin Surg Oncol.* 1997;13:190-195.

(31) Nag S. The evolving role of brachytherapy in breast cancer. *Am J Clin Oncol.* 18[4], 353-357.

(32) Veronesi U, Salvadori B, Luini A et al. Breast conservation is a safe method in patients with small cancer of the breast. Long-term results of three randomised trials on 1,973 patients. *Eur J Cancer.* 1995;31A:1574-1579.

(33) Arthur, D. W. Accelerated Partial Breast Irradiation: A Change In Treatment Paradigm for Early Stage Breast Cancer. *Journal of Surgical Oncology* 84[4], 185-191. 2003.

(34) Arthur DW, Koo D, Zwicker RD et al. Partial breast brachytherapy after lumpectomy: low-dose-rate and high-dose-rate experience. *Int J Radiat Oncol Biol Phys.* 2003;56:681-689.

(35) Vicini FA, Arthur DW. Breast brachytherapy: North American experience. *Semin Radiat Oncol.* 2005;15:108-115.

(36) Polgar C, Major T. Current status and perspectives of brachytherapy for breast cancer. *Int J Clin Oncol.* 2009;14:7-24.

(37) Patel RR, Arthur DW. The emergence of advanced brachytherapy techniques for common malignancies. *Hematol Oncol Clin North Am.* 2006;20:97-118.

(38) Trombetta M, Julian T, Bhandari T, Werts ED, Miften M, Parda D. Breast conservation surgery and interstitial brachytherapy in the management of locally recurrent carcinoma of the breast: the Allegheny General Hospital experience. *Brachytherapy.* 2008;7:29-36.

(39) Swanson TA, Vicini FA. Overview of accelerated partial breast irradiation. *Curr Oncol Rep.* 2008;10:54-60.

(40) Aristei C, Tarducci R, Palumbo I et al. Computed tomography for excision cavity localization and 3D-treatment planning in partial breast irradiation with high-dose-rate interstitial brachytherapy. *Radiother Oncol.* 2009;90:43-47.

(41) Cuttino LW, Todor D, Arthur DW. CT-guided multi-catheter insertion technique for partial breast brachytherapy: reliable target coverage and dose homogeneity. *Brachytherapy.* 2005;4:10-17.

(42) Dickler A, Kirk MC, Chu J, Nguyen C. The MammoSite breast brachytherapy applicator: a review of technique and outcomes. *Brachytherapy.* 2005;4:130-136.

(43) Strauss JB, Dickler A. Accelerated partial breast irradiation utilizing balloon brachytherapy techniques. *Radiother Oncol.* 2009;91:157-165.

(44) Fentiman IS, Poole C, Tong D et al. Iridium implant treatment without external radiotherapy for operable breast cancer: a pilot study. *Eur J Cancer.* 1991;27:447-450.

(45) DA Wilkinson. High dose rate (HDR) brachytherapy quality assurance: a practical guide. *Biomedical Imaging and Intervention Journal* 2[2], e34. 2006.

APPENDIX A: MATLAB CODE

Reading five DICOM images for a single dwell position.

```
cd('C:\BBs_projections\HDR Tracking');  %set the working directory to the
file where the DICOM image data is stored
[FileName,PathName] = uigetfile('*.*','select first image');  %displaying
a modal dialogue box with a message to select the first image from the
directory cd
cd(PathName)   %set the working directory to the first DICOM image data
info = dicominfo(FileName);  %reads the matadata from the DICOM file
X1 = dicomread(info);    %reads the image data from the DICOM file
```

Similarly the 2nd 3rd 4th and 5th image are read and stored in X2, X3, X4 and X5 respectively.

```
X6 = (X1 + X2 + X3 + X4 + X5);  %image averaging

X7 = X6./5;
```

The blank image is read and saved in X8 and subtracted from X7

```
X = X7 - X8; %subtracting the blank image from the averaged image
```

Image processing, Isolating and Labeling markers, Calculating Centroid

```
I=X(26:743,26:999);  %cropping the image
se = strel('disk',25);  %morphological bottom hat filter
I1 = imbothat(I,se);
[I2,noise] = wiener2(I1,[15 15]);  %noise removal filter
I3 = medfilt2(I2,[8 8]);
I4 = I3>mean2(I3) + 2.5*std2(I3); %applying threshold to convert the
image to binary
[I5,NUM] = bwlabeln(I4);  %labeling the markers
STATS = regionprops(I5,'Centroid','Area');  %calculating the centroid
n = length(STATS);

for i = 1:n
    areas(i)=STATS(i).Area;
    xx(i) = STATS(i).Centroid(1);
    yy(i) = STATS(i).Centroid(2);
    xx1(i) = 0.0388*(xx(i)-487);
    yy1(i) = 0.0388*(359 - yy(i));

end;
```

Sorting the labeled markers

```
[cent_y,IM_y] = sort(yy);
n = 1;
img = [];
for i = 1:5
    IMG1 = IM_y(n:n+7);
    IMG2 = sort(IMG1);
    img = [img IMG2];
    n = n + 8;
end
```

The calibration image is read and saved in X9

Image processing for calculating centroids for the calibration image

```
I6=X9(26:743,26:999);
se = strel('disk',25);
I7 = imbothat(I6,se);
[I8,noise] = wiener2(I7,[15 15]);
I9 = medfilt2(I8,[8 8]);
I10 = I9>mean2(I9) + 2.5*std2(I9);
[I11,NUM] = bwlabeln(I10);
STATS1 = regionprops(I11,'Centroid','Area');
n = length(STATS1);
for i = 1:n
    areas(i)=STATS1(i).Area;
    xx2(i) = STATS1(i).Centroid(1);
    yy2(i) = STATS1(i).Centroid(2);
    xx3(i) = 0.0388*(xx2(i) - 487);
    yy3(i) = 0.0388*(359 - yy2(i));

end;
```

Sorting the labeled markers

```
[cent_y,IM_y] = sort(yy2);
n = 1;
cal = [];
for i = 1:5
    IMG1 = IM_y(n:n+7);
    IMG2 = sort(IMG1);
    cal = [cal IMG2];
    n = n + 8;
end
```

Calculating 3D coordinates of the markers

```
Final_pt = [0 0 150];
t = 25.49/150;
n = length(STATS1);
for i = 1:n
    Initial_pt = [xx3(i),yy3(i),0];
    r = Final_pt - Initial_pt;
    x(i) = xx3(i) + t*r(1);
    y(i) = yy3(i) + t*r(2);
end
```

Model for calculating the 3D coordinates of the HDR source

```
n = length(img);
D = [];                                  %declaring variables
Px = []; Py = []; Pz = [];
Qx = []; Qy = []; Qz = [];
P = {}; Q = {}; DD = {};
imageX = []; imageY = []; calX = []; calY = [];

for i = 1:n
    p1 = [xx1(img(i)) yy1(img(i)) 0];
    p2 = [x(cal(i)) y(cal(i)) 25.49]; % paring 1st marker with its
projection

    imageX = [imageX xx1(img(i))];
    imageY = [imageY yy1(img(i))];
    calX = [calX x(cal(i))];
    calY = [calY y(cal(i))];

    for ii = i+1:n
        p3 = [xx1(img(ii)) yy1(img(ii)) 0];
        p4 = [x(cal(ii)) y(cal(ii)) 25.49]; % paring 1st marker with its
projection
```

```
%model for calculating P, Q, D … the process is repeated for every marker
projection pair

        p13(1) = p1(1) - p3(1);
        p13(2) = p1(2) - p3(2);
        p13(3) = p1(3) - p3(3);

        p43(1) = p4(1) - p3(1);
        p43(2) = p4(2) - p3(2);
        p43(3) = p4(3) - p3(3);

        if ((abs(p43(1))  < eps) & ...
           (abs(p43(2))  < eps) & ...
           (abs(p43(3))  < eps))
           error('Could not compute LineLineIntersect!');
        end

        p21(1) = p2(1) - p1(1);
        p21(2) = p2(2) - p1(2);
        p21(3) = p2(3) - p1(3);

        if ((abs(p21(1))  < eps) & ...
           (abs(p21(2))  < eps) & ...
           (abs(p21(3))  < eps))
           error('Could not compute LineLineIntersect!');
        end

        d1343 = p13(1) * p43(1) + p13(2) * p43(2) + p13(3) * p43(3);
        d4321 = p43(1) * p21(1) + p43(2) * p21(2) + p43(3) * p21(3);
        d1321 = p13(1) * p21(1) + p13(2) * p21(2) + p13(3) * p21(3);
        d4343 = p43(1) * p43(1) + p43(2) * p43(2) + p43(3) * p43(3);
        d2121 = p21(1) * p21(1) + p21(2) * p21(2) + p21(3) * p21(3);

        denom = d2121 * d4343 - d4321 * d4321;

        if (abs(denom) < eps)
           error('Could not compute LineLineIntersect!');
        end

        numer = d1343 * d4321 - d1321 * d4343;

        mua = numer / denom;
        mub = (d1343 + d4321 * mua) / d4343;

        pa(1) = p1(1) + mua * p21(1);
        pa(2) = p1(2) + mua * p21(2);
        pa(3) = p1(3) + mua * p21(3);
        pb(1) = p3(1) + mub * p43(1);
        pb(2) = p3(2) + mub * p43(2);
        pb(3) = p3(3) + mub * p43(3);
```

```
        pd = pa-pb;
        d = sqrt((pd(1)*pd(1)) + (pd(2)*pd(2)) + (pd(3)*pd(3)));

        D = [D d];
        Px = [Px pa(1)];
        Py = [Py pa(2)];
        Pz = [Pz pa(3)];
        Qx = [Qx pb(1)];
        Qy = [Qy pb(2)];
        Qz = [Qz pb(3)];

        P{i,ii} = pa;      Q{i,ii} = pb;      DD{i,ii} = d;

    end
end

PP = [mean(Px) mean(Py) mean(Pz)]  %calculating and displaying P
stdP = [std(Px) std(Py) std(Pz)]
QQ = [mean(Qx) mean(Qy) mean(Qz)]  %calculating and displaying Q
stdQ = [std(Qx) std(Qy) std(Qz)]
meanD = mean(D)                    %calculating and displaying D
stdD = std(D)
PQ = (PP+QQ)/2                     %calculating and displaying the HDR
source position
```

APPENDIX B: File From the Planning System Containing the 3D Coordinates of the Treatment Plan

info =

Filename: 'RP.1.2.246.352.71.5.2095773342.135265.20100406155112.dcm'
FileModDate: '09-Apr-2010 13:11:18'
FileSize: 15494
Format: 'DICOM'
FormatVersion: 3
Width: []
Height: []
BitDepth: []
ColorType: ''
FileMetaInformationGroupLength: 164
FileMetaInformationVersion: [2x1 uint8]
MediaStorageSOPClassUID: '1.2.840.10008.5.1.4.1.1.481.5'
MediaStorageSOPInstanceUID: '1.2.246.352.71.5.2095773342.135265.20100406155112'
TransferSyntaxUID: '1.2.840.10008.1.2'
ImplementationClassUID: '1.2.246.352.70.2.1.7'
SpecificCharacterSet: 'ISO_IR 100'
InstanceCreationDate: '20100409'
InstanceCreationTime: '130958'
SOPClassUID: '1.2.840.10008.5.1.4.1.1.481.5'
SOPInstanceUID: '1.2.246.352.71.5.2095773342.135265.20100406155112'
StudyDate: '20100406'
StudyTime: '131634'
AccessionNumber: ''
Modality: 'RTPLAN'
Manufacturer: 'Varian Medical Systems'
ReferringPhysicianName: [1x1 struct]
StationName: 'RO-ARIA'
SeriesDescription: 'ARIA RadOnc Plans'
OperatorName: [1x1 struct]
ManufacturerModelName: 'Aria RadOnc'

PatientName: [1x1 struct]
PatientID: '0404040404040404'
PatientBirthDate: ''
PatientSex: ''
DeviceSerialNumber: '2095773342'
SoftwareVersion: '8.6.15'
StudyInstanceUID: '1.2.840.113704.1.111.2440.1270565981.10'
SeriesInstanceUID: '1.2.246.352.71.2.2095773342.582043.20100406154828'
StudyID: '11293'
SeriesNumber: 4
FrameOfReferenceUID: '1.2.840.113704.1.111.6128.1270574230.4'
PositionReferenceIndicator: ''
RTPlanLabel: 'Plan1'
RTPlanDate: '20100406'
RTPlanTime: '162256'
RTPlanGeometry: 'PATIENT'
FractionGroupSequence: [1x1 struct]
BrachyTreatmentTechnique: 'INTERSTITIAL'
BrachyTreatmentType: 'HDR'
TreatmentMachineSequence: [1x1 struct]
SourceSequence: [1x1 struct]
ApplicationSetupSequence: [1x1 struct]
ReferencedStructureSetSequence: [1x1 struct]
ApprovalStatus: 'UNAPPROVED'

The 3D coordinates for the plan is contained in info. ApplicationSetupSequence

The applicator number are contained in
Info.ApplicationSetupSequence.Item_1.ChannelSequence

Item_1: [1x1 struct]
Item_2: [1x1 struct]

Item_1 contains information on the 1st applicator and Item_2 contains information on the 2nd applicator

Info.ApplicationSetupSequence.Item_1.ChannelSequence.Item_1

ReferencedROINumber: 2
NumberOfControlPoints: 60
ChannelNumber: 1
ChannelLength: 1500
ChannelTotalTime: 300.0000
SourceMovementType: 'STEPWISE'
SourceApplicatorNumber: 1
SourceApplicatorID: 'Applicator1'
SourceApplicatorType: 'RIGID'
SourceApplicatorLength: 1500
SourceApplicatorStepSize: 5
TransferTubeNumber: ''
FinalCumulativeTimeWeight: 300.0000
BrachyControlPointSequence: [1x1 struct]
ReferencedSourceNumber: 1

The 3D coordinates for the 1st position of the 1st applicator is contained in info.ApplicationSetupSequence.Item_1.ChannelSequence.Item_1.BrachyControlPointSequence.Item_1.ControlPoint3DPosition

Similarly the 3D coordinates of all the source positions can be obtained.

VITA

Aditya Bondal was born in Mumbai, India on 11th September 1983 and is currently the citizen of India. He completed his high school from Don Bosco High School, Matunga in 1999. In June 2006, Aditya received his Bachelors degree in Instrumentation Engineering from Mumbai University, India. In fall 2006 he started his graduate studies with Virginia Commonwealth University in Biomedical Engineering. During this time he worked as a Teaching Assistant in the School of Engineering and is currently working as a Research Assistant in the department of Radiation Oncology. He has presented various posters including the American Association of Physicists in Medicine (AAPM). In 2009 Aditya was the finalists for the Young Investigators Symposium at the AAPM conference held in Anaheim, CA.